Conformational flexibility of HIV-1 envelope glycoproteins modulates transmitted / founder sensitivity to broadly neutralizing antibodies

Sneha Ratnapriya[1,10], Karunakar Reddy Pothula[3,10], Kim-Marie A. Dam[2,10], Durgadevi Parthasarathy[1,10], Héctor Cervera Benet[1], Ruth Parsons[3], Xiao Huang[3], Salam Sammour[3], Katarzyna Janowska[3], Miranda Harris[1], Shamim Ahmed[1], Samuel Sacco[2,11], Joseph Sodroski[4], Michael D. Bridges[5,6], Wayne L. Hubbell[5,6], Priyamvada Acharya[3,7] and Alon Herschhorn[1,8,9]*

[1]Division of Infectious Diseases and International Medicine, Department of Medicine, University of Minnesota, Minneapolis, MN, USA

[2]Division of Biology and Biological Engineering, California Institute of Technology, Pasadena, CA, USA

[3]Duke Human Vaccine Institute, Durham, NC, USA

[4]Department of Cancer Immunology and Virology, Dana-Farber Cancer Institute, Boston, MA, USA; Department of Microbiology, Harvard Medical School, Boston, MA, USA

[5]Jules Stein Eye Institute, University of California, Los Angeles, CA, USA

[6]Department of Chemistry and Biochemistry, University of California, Los Angeles, CA, USA

[7]Department of Surgery, and Department of Biochemistry, Duke University, Durham, NC, USA

[8]Institute for Molecular Virology, University of Minnesota, Minneapolis, MN, USA

[9]Microbiology, Immunology, and Cancer Biology Graduate Program; The College of Veterinary Medicine Graduate Program; and the Molecular Pharmacology and Therapeutics Graduate Program, University of Minnesota, Minneapolis, MN, USA

[10]These authors contributed equally: Sneha Ratnapriya, Karunakar Reddy Pothula, Kim-Marie A. Dam, and Durgadevi Parthasarathy

[11]Present address: Department of Ecology and Evolutionary Biology, University of California Santa Cruz, Santa Cruz, CA, USA

*Correspondence:
Alon Herschhorn
Room 2-101 MRF
689 23rd Av SE
University of Minnesota
Minneapolis, MN 55455
Email: aherschh@umn.edu
Phone: 612-3012429

Abstract

HIV-1 envelope glycoproteins (Envs) mediate viral entry and are the sole target of neutralizing antibodies. Envs of most primary HIV-1 strains exist in a closed conformation and occasionally sample more open Env states. Thus, current knowledge guides immunogen design to mimic the closed Env conformation as the preferred target for eliciting broadly neutralizing antibodies (bnAbs) to block HIV-1 entry. Here we show that Env-preferred conformations of 6 out of 13 (46%) transmitted/founder (T/F) strains tested are incompletely closed. As a result, entry of these T/Fs into target cells is sensitive to antibodies that recognize internal epitopes exposed on open Env conformations. A cryo-electron microscopy structure of unliganded, incompletely closed T/F Envs (1059-SOSIP) at 3.6 Å resolution exhibits an asymmetric configuration of Env protomers with increased sampling of states with incompletely closed trimer apex**.** An additional structure of the 1059-SOSIP complexed with the CD4-induced antibody 17b without the requirement for prior sCD4 binding, together with double electron-electron resonance spectroscopy, provided further evidence for enriched occupancy of more open conformations. 1059 Env conformational flexibility was associated with resistance to bnAbs that preferentially neutralize the closed Env conformation. To follow the fate of incompletely closed Env in patients, we reconstructed *de novo* the post-transmission evolutionary pathway of a second T/F Env (CH040), which is sensitive to the V3-targeting antibody 19b and highly resistant to most bnAbs. Evolved viruses exhibited increased resistance to cold, soluble CD4 and 19b, all of which correlate with the evolution of a more closed Env state. Lastly, we show a correlation between efficient neutralization of multiple Env conformations and increased antiviral breadth of CD4-binding site (CD4bs) bnAbs. In particular, N6 CD4bs bnAb, which uniquely recognizes different Env conformations, efficiently neutralizes 50% of the HIV-1 strains that were resistant to VRC01 and transmitted during the first-in-humans antibody-mediated prevention trial (HVTN 704). VRC01-resistant Envs are incompletely closed based on their sensitivity to cold and on partial sensitivity to antibodies targeting internal epitopes, which are typically occluded in tightly closed Envs. Most VRC01-resistant Envs retain the VRC01 epitope according to VRC01 binding to their gp120 subunit at concentrations that have no significant effect on virus entry, and they exhibit cross resistance to other CD4bs bnAbs that preferentially neutralize the closed Env conformation. Our findings refine current knowledge of Env conformational states and provide guidance for developing new strategies for bnAb immunotherapy and Env-based immunogen design.

Main

Interaction of HIV-1 envelope glycoproteins (Envs) with the cellular CD4 receptor and CCR5/CXCR4 coreceptor mediates virus entry into target cells[1–5]. HIV-1 Envs are expressed on the surface of HIV-1 virions as trimeric spikes, with each spike composed of three gp120 exterior glycoproteins non-covalently associated with three gp41 transmembrane glycoproteins[6]. HIV-1 Env trimers of most primary isolates prefer to adopt a metastable closed, pre-fusion conformation and transit, either spontaneously or once they bind the CD4 receptor, to downstream conformations[7]. Transition to an open conformation is mediated by extensive structural rearrangements that result in: a) outward displacement of the gp120 V1/V2 from the apex to the sides of the trimer; b) exposure of V3 loop that becomes disordered but appears to stay at the trimer apex; c) formation of a 4-stranded bridging sheet that connects the outer and inner domains of gp120, d) exposure of the coreceptor-binding site (-bs)[8–15] and (e) structural changes at the gp120/gp41 interface that alter access to the gp41 fusion peptide[16,17] . Cryo-EM structures of soluble BG505 and B41 SOSIP Env trimers, which were stabilized in an open conformation by a combination of soluble CD4 (sCD4) and a CD4-induced antibody, showed that the carboxyl terminus of gp41 heptad repeat 1 (HR1) becomes compact while additional helical turns form at the $HR1_C$ N terminus[13,17]. While there are no structures yet that show complete exposure of gp41 HR1 on the Env surface upon CD4 binding, HR1-specific ligands (i.e., C34 and T20 peptides) bind surface-expressed Envs after interaction with sCD4, suggesting that gp41 HR1 coiled coil is exposed on a CD4-bound Env trimer[18–20]. Subsequent engagement of the Env-CD4 complex with the CCR5 or CXCR4 coreceptor moves the Envs down the energy gradient on the entry pathway, culminating in the formation of a gp41 six-helix bundle that facilitates the fusion of viral and cellular membranes[21–24].

Functional, entry-compatible intermediates of HIV-1 Envs can be enriched by introducing amino acid changes in control residues (e.g., L193A) that are highly conserved across all clades and restrain Envs in a closed conformation in primary wild-type isolates[7,25]. Functional Env intermediates are associated with hypersensitivity to cold[7,18,25] and to some but not all ligands that recognize internal epitopes, which are only exposed on more open Env conformations (e.g., sCD4, antibodies such as 17b, 19b, E51, and T20 peptide). Thus, sensitivity of HIV-1 to different Env ligands can identify exposure of internal epitopes on the Env surface and serves to define different Env conformations (closed, incompletely closed, intermediate, and open). Based on this concept, several studies have provided evidence that the Envs of some primary HIV-1 strains may preferentially adopt a more open conformation relative to other primary isolates[26–28]. For example, some antibodies directed against the V3 loop of gp120 (e.g., 19b) neutralize only HIV-1 that exhibit partially or completely open Env conformations, which expose the V3 loop[7]. Unexpectedly, these antibodies neutralize a subset of global, “difficult-to-neutralize” HIV-1 isolates as well as a minority of transmitted/founder (T/F) strains, which can establish *in vivo* HIV-1 infection[26,27]. Here we developed a highly sensitive approach to assess HIV-1 Env conformational flexibility and heterogeneity by using different Env ligands and identified T/F Envs that preferentially exist in an incompletely closed conformation. We solved the cryo-EM structure of an unliganded, incompletely closed T/F (1059) SOSIP Env and identified structural determinants of protomer flexibility and increased sampling of incompletely closed states. We further solved the structure of 1059 SOSIP in complex with the CD4-induced antibody 17b[29] and

measured the distance distributions of Env conformations using double electron-electron resonance (DEER) spectroscopy[30]. To follow the fate of incompletely closed Envs *in vivo*, we reconstructed viruses at different time points during in-patient evolution based on consensus HIV-1 sequences for each time point. Lastly, we associated the ultra-broad and potent neutralizing activity of the CD4-binding site (CD4bs) bnAb N6 (ref[31]) with recognition of closed and open Env conformations; we then evaluated the antiviral activity of N6 against VRC01-resistant strains with incompletely closed Envs isolated from the first-in-humans antibody-mediated prevention trial (HVTN 704).

HIV-1 Envs of some T/F strains can adopt an incompletely closed conformation and resist bnAb neutralization

To define the contribution of different elements to opening of Env conformation, we generated 53 functional Env variants by introducing changes in control residues that restrain the closed Env conformation of HIV-1_{JR-FL}. We specifically designed a panel of Env variants containing the L193A and I423A changes, which were identified in our previous studies[7,18,25], to enrich functional intermediates in this group. All Env intermediates were functional with an average infectivity of 243% in comparison with WT JR-FL (Cf2-Th/$CD4^+CCR5^+$ target cells; range 3% - 2084%; Supplementary Table 1). We tested HIV-1 sensitivity to Env ligands and identified variants with >10-fold increase in sensitivity to ligands that recognize internal elements associated with more open Env conformations (sCD4, CD4-induced Ab 17b, V3-directed Ab 19b, V1/V2-directed Ab 902090, and gp41 HR1-directed T20 peptide; Fig. 1a and Supplementary files: Table 1 & Fig. 1). Analysis of the neutralization sensitivity of these 53 Env intermediates allowed us to map specific Env sites that are substantially exposed. We found that the gp120 V3 loop was the most frequently exposed element. In addition, among intermediates that exposed only a single Env element, V3 was the most frequently exposed; by contrast, none of the variants exposed only coreceptor-bs or only the V1/V2 loop (Supplementary Table 1). These observations suggest that in many cases the V3 loop may be the first element to be exposed during the opening of the Env trimer. Based on our results, we conclude that functional, entry-compatible HIV-1 Envs can expose single or different internal domains.

We next used these tools to analyze exposure of different sites on a panel of T/F Envs. HIV-1 T/Fs represent a subset of viral strains that can cross the mucosal bottleneck and establish HIV-1 infection in humans, making them a main target of a preventive HIV-1 vaccine[27,32]. T/F virions display on their surface ~1.9-fold more Envs compared with chronic HIV-1 isolates and they are highly resistant to antiviral activity of α and β interferons[32,33]. We selected 13 previously published T/F Envs[27] (Extended Data Table 2), which exhibited high infectivity *in vitro* (>10^6 relative light units), and tested their sensitivity to antibodies that recognize internal Env elements (E51,17b, 39F, 19b, 697-30D, F105, T20, 240-D, and 246D; Fig. 1b-d and Extended Data Fig. 1). We identified 6 T/F Envs (46%) that were inhibited by >50% by at least one antibody. These Envs could be clustered into 3 groups: Group 1 included CH040, 1058 and 9021 Envs that exposed only the V3 loop based on 19b sensitivity; Group 2 included SC45 and 1059 Envs that exposed the V3 loop and epitopes of the coreceptor-bs based on sensitivity to E51, 17b and 39F (1059 was only weakly sensitive to 17b); and Group 3 included WEAU Envs that exposed many

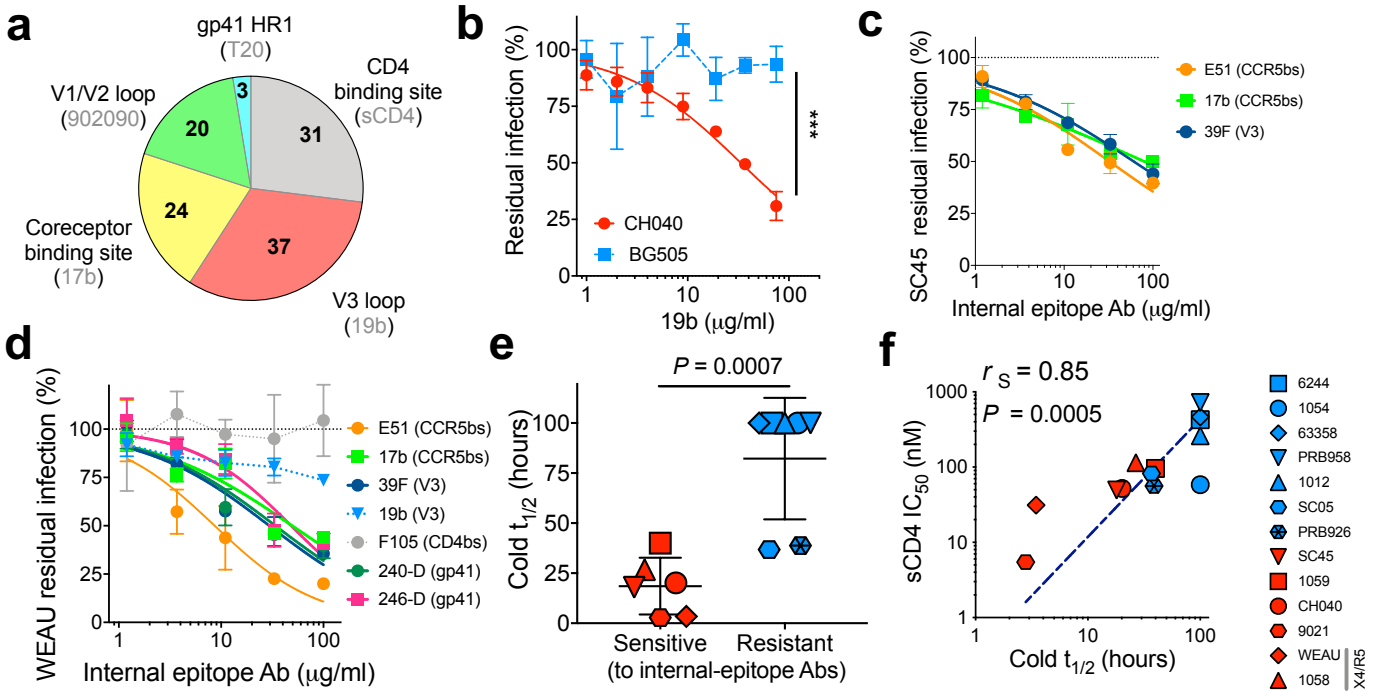

Figure 1. Incompletely closed Env conformation of transmitted/founder (T/F) strains. a, We measured the sensitivity of WT and 53 selected HIV-1_{JRFL} Env variants, which are enriched (not randomly selected) in intermediates, to ligands that recognize internal Env epitopes (sCD4; 17b, 19b, 902 antibodies; and T20 peptide) and calculated the contribution of each HIV-1 Env site exposure to trimer opening (number of variants hypersensitive to the specified antibodies; Supplementary Table 1 and Supplementary Fig. 1). **b-d,** Sensitivity of CH040 (**b**), SC45 (**c**), and WEAU (**d**) Envs to different antibodies recognizing internal epitopes. BG505 was used as a control in (**b**). **e**, Relationship between T/F Env sensitivity to internal-epitope antibodies and the sensitivity to cold. *P,* two-tailed Student's t-test P value. **f,** Relationship between cold and sCD4 sensitivities of T/F Envs that are sensitive (red) or resistant (blue) to internal-epitope antibodies. Dashed line is a log/log fit curve. r_S, Spearman correlation coefficient; *P*, P value for calculated correlation coefficient. Strain IDs in panels **e** and **f** are identical and shown on the right.

internal epitopes, including cluster I epitopes of gp41 (Fig.1b-d and Extended Data Fig. 1). Similar to our results with the 53 HIV-1_{JR-FL} variants, the V3 loop was the most frequently exposed Env element but T/F Envs were only weakly to moderately sensitive to internal-epitope antibodies, indicating that subset of Envs are incompletely closed and only slightly or temporarily expose internal epitopes. Consistent with an incompletely closed Env conformation, neutralization-sensitive viruses were significantly (*P*=0.0007) more sensitive to cold exposure (Fig. 1e and Extended Data Fig. 2a-b) than the remaining T/F viruses in this group. More open Env conformations are more sensitive to inactivation in the cold[7,18,34]. T/F viruses with incompletely closed Envs were also more sensitive to sCD4, although this difference did not reach statistical significance (*P*=0.05; Extended Data Fig. 2d); and we observed a significant correlation between cold and sCD4 sensitivity (*P*=0.0005; Fig. 1f). Notably, two out of two dual-tropic (X4/R5) Envs (1058 and WEAU) in the T/F group were incompletely closed and hypersensitive to cold and sCD4. We next measured T/F virus sensitivity to bnAbs directed against known sites of Env vulnerability and detected diverse patterns of susceptibility (Extended Data Fig. 3). We focused on 1059 Envs because viruses pseudotyped with these Envs were hypersensitive to bnAbs directed against the gp41 membrane-

proximal external region (MPER), which preferentially neutralize more open Env conformations[7,35–37] and were highly resistant to VRC01, VRC03, 3BNC117, and PG9 (but not PGT145) bnAbs that preferentially recognize closed Env conformations[7,36] (Extended Data Fig. 3). Of note, 1059 Envs contain the I169, D279, and E471 amino acids that are associated with resistance of some HIV-1 strains to V1/V2-targeting, VRC03 and VRC01 bnAbs, respectively. However, these residues are not sufficient for HIV-1 resistance as other HIV-1 strains that contain the same amino acids at these positions such as T/F WITO and REJO (containing I169) exhibit high bnAb sensitivity[38]. To evaluate the integrity of bnAb epitopes in 1059 Envs we tested bnAb binding to soluble 1059 gp120, in which the CD4bs is fully accessible to antibodies. Despite resistance of 1059 Env trimers on virions to several CD4bs bnAbs, soluble 1059 gp120 strongly bound VRC01 and to a lesser extent 3BNC117, and this binding was comparable to the binding of these antibodies to gp120 of AD8, an HIV-1 strain which is hypersensitive to neutralization by CD4bs and V1V2 bnAbs (Extended Data Fig. 4a-d). In contrast, soluble 1059 gp120 only weakly-moderately bound VRC03. Thus, resistance of 1059 Envs to VRC01 and 3BNC117 is consistent with a conformational effect that limits target site accessibility in the context of the native Env trimer, whereas resistance to VRC03 may be related to a combined effect of epitope integrity and accessibility. Resistance of 1059 Envs to PG9 but not PG145 suggests a local effect. Both bnAbs target V1/V2 quaternary epitopes and therefore poorly bind soluble gp120. Nevertheless, binding of both bnAbs to 1059 gp120 was comparable to or stronger than their binding to AD8 gp120 (Extended Data Fig. 4c). In comparison with a virus with tightly closed Envs (e.g., BG505), the incompletely closed 1059 Envs required lower concentrations of exogenous sCD4 to infect Cf2-Th/CCR5^{+} target cells (Extended Data Fig. 4e).

HIV-1_{1059} Env resists VRC01 neutralization despite strong binding of soluble monomeric 1059 gp120 to VRC01 (Extended Data Fig. 4a-d), suggesting interference with access of VRC01 to its binding site on the native HIV-1_{1059} Envs on virions. To gain insights into the structural features of the incompletely closed Env identified in this screen, we determined cryo-EM structures of 1059 SOSIP, and for comparison, of the well-characterized BG505-SOSIP variant. Both the 1059- and BG505-SOSIP trimers were purified using *Galanthus nivalis* lectin chromatography, which exploits lectin binding to Env surface glycans in a conformation-independent manner, followed by size-exclusion chromatography (SEC; Extended Data Figs. 5 & 6). We obtained cryo-EM reconstructions of unliganded 1059-SOSIP, resolved at 3.6 Å with 737,588 particles, and of BG505-SOSIP resolved at 3.7 Å with 975,399 particles. To assess variability in the datasets, we further classified each particle stack into 10 sub-classes. Analysis of the unliganded 1059-SOSIP sub-classes revealed three structural characteristics of the incompletely closed Envs (Fig. 2a-d): 1. conformational flexibility 2. asymmetry and 3. partial opening of trimer apex. Within these 10 subclasses, we observed a larger range of protomer motion in 1059-SOSIP compared with the limited range of motion observed in BG505-SOSIP (Fig. 2b and Extended Data Fig. 7a). The 10 sub-classes obtained for 1059-SOSIP showed variable levels of asymmetry in the protomer arrangement that were significantly greater (P value = 0.0019; Fig. 2c, Extended Data Fig. 7b and Extended Data Table 4) than the asymmetry observed in the BG505-SOSIP subclasses. Further, 3D variability analysis of 1059-SOSIP captured scissoring motion of the protomers, and partial opening of the trimer characterized by outward motion of V1/V2 loop from the trimer apex (Fig. 2d; Supplementary Movies 1 and 2, PC1 and PC3). In

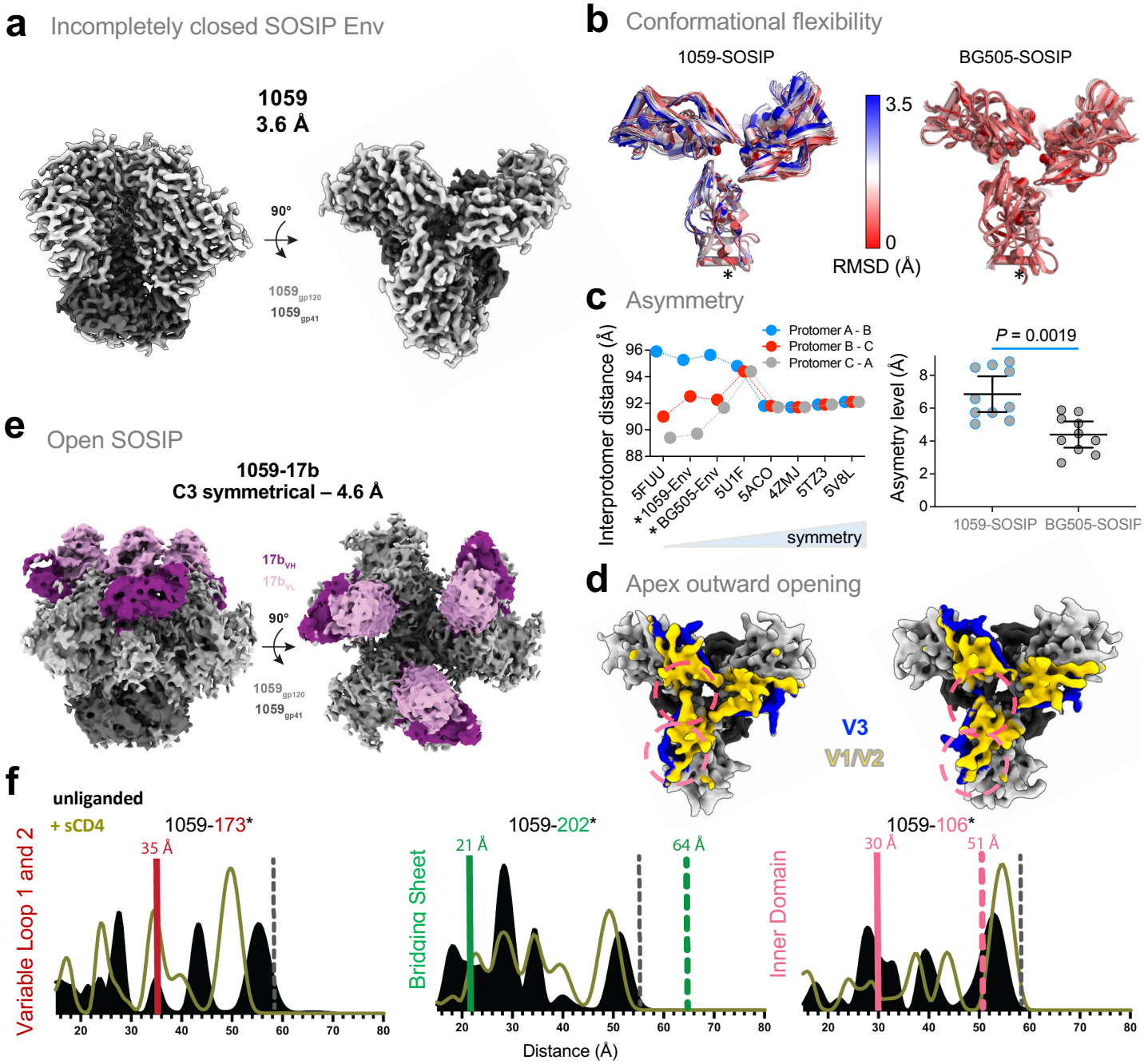

Figure 2. Cryo-EM structure and conformation of incompletely closed SOSIP Envs of a transmitted / founder (1059) HIV-1 strain. a, Side and top views of unliganded incompletely closed 1059-SOSIP structure at 3.6 Å. **b-d,** Structural determinants of incompletely closed SOSIP. **b,** Conformational flexibility**.** Overlay of 10 rigid fitted sub-class models of 1059 or BG505 SOSIPs purified and analyzed under identical conditions. Color bar indicates the C-alpha root mean square deviation between those structures. We used one protomer (noted with an asterisk) for superposition and calculated the C-alpha root the mean deviation between the structures. Number of particles used, and resolution of each sub-class model are provided in Extended Data Table 4. **c,** Asymmetry. We measured the inter-protomer distances between residues 343 of gp120 α2 helix of different protomers in each structure to assess asymmetry. **Left,** interprotomer distances of different soluble Envs, including 2 asymmetric structures (PDB: 5FUU & 5U1F) that were obtained with cryo-EM and refined with C1 symmetry and four symmetric structures (PDB: 4ZMJ, 5ACO, 5TZ3 and 5V8L) that were obtained either by X-ray crystallography or by cryo-EM and refined with C3 symmetry except the 5V8L. *, SOSIP structures solved in this study by cryo-EM and refined with C1 symmetry. **Right,** a statistical analysis of the difference in asymmetry level between the 1059 and BG505 SOSIPs calculated from the 10 respective subclasses for each SOSIP. Asymmetry was calculated based on deviation from inter-protomer distances as described in Methods. *P,* two-tailed *P* value of Mann-Whitney U-test. **d,** Mobility. CryoSPARC 3D variability analysis revealed disruption of the trimer apex and outward movement of the V1/V2 loop (also see Supplementary Movies, principal component 3 motion). Two snapshots are shown where the V1/V2 loop (yellow) is shifting outward from the trimer (pink circles). **e,** A structure of open 1059-SOSIP when in complex with 17b. **f,** DEER spectroscopy data for interprotomer distance distributions for V1 spin labels in V1V2 (residue 173), bridging sheet

(residue 202), and inner domain (residue 106) for unliganded and sCD4-bound 1059 SOSIPs. Vertical solid and dashed lines represent interprotomer Cα distance measurements at target sites for closed (PDB: 5T3Z) and sCD4-liganded (PDB: 5VN3) structures, respectively. Residue 173 was disordered for sCD4-Env structure (distance not shown). Grey dotted line indicates the upper limit for reliably measuring distances using DEER technology. SOSIP trimers were purified by GNL/SEC (**a-d**) or 2G12 Ab/SEC (**e-f**).

with the lower range of protomer motion observed for BG505-SOSIP, the 3D variability analysis of BG505-SOSIP, revealed no significant opening motions of the SOSIP trimer. Overall, the 1059-SOSIP cryo-EM analysis reveals occupancy of a wider range of protomer conformations contributing to augmented outward motion of the V1/V2 loop at the trimer apex and higher asymmetry of the Env trimer, compared to BG505-SOSIP. Notably, both 1059-SOSIP and antibody PGT151 bound JRFL Env (PDB ID: 5FUU) structures are asymmetric, clustered together in a principal component analysis (Extended Data Fig. 7d) and exhibited promoter scissoring. To assess whether the conformational flexibility of 1059-SOSIP facilitates direct transitions to the open Env state we solved the structure of 1059-SOSIP (purified by 2G12 followed by SEC) in complex with17b Fab. Based on ELISA, binding of 1059 SOSIP to 17b in the absence of sCD4 was strong, whereas binding of the control BG505 SOSIP to 17b could be detected only in the presence of sCD4 (Extended Data Fig. 5). At 4.7 Å resolution (with C3 symmetry, which was identified in the map, applied during map reconstruction), the cryo-EM reconstruction of 1059-SOSIP-17b complex exhibited an open Env conformation and could fit to structures of SOSIP trimers complexed with sCD4 and 17b (Fig. 2e and Extended Data Fig. 9). This is the first structure showing CCR5-bs exposure on the Env from a T/F strain in the absence of sCD4 or a CD4 mimetic. In the presence of 17b, we also detected a minor subset of particles that contained unliganded 1059 SOSIP but the moderate resolution of 4.7 Å (with C3 symmetry, which was identified in the map, applied during reconstruction) precluded detailed analysis of this structure (Extended Data Fig. 9).

To evaluate the distribution of different Env conformations of an incompletely closed SOSIP Envs, we used DEER spectroscopy[39–41]. A nitroxide spin label with a V1 side chain was covalently attached to a free cysteine that was introduced into a gp120-gp41 protomer, as previously described for DEER studies of SOSIP trimers[30] (Fig. 2f and Extended Data Fig. 10). This attachment results in three labels per Env SOSIP, allowing inter-protomer distance measurements that can differentiate between Envs that exhibit homogeneous conformation profiles (represented by a single dominant distance distribution) and Envs that exhibit heterogeneous conformation profiles (represented by multiple, sub-dominant distance measurements)[30]. For some spin label placements, distance measurements can be correlated to closed and open SOSIP conformations defined by inter-protomer Cα-Cα distance measurements between protomers on published structures of SOSIP Envs. Longer distances than the predicted-closed-SOSIP-conformation distances are associated with more open Env conformations. To understand the conformational profile of 1059 Env, we labeled gp120 sites in the V1V2 loop (173*; (*, nitroxide spin label)), bridging sheet (202*), and inner domain (106*). 1059 SOSIP showed more conformational heterogeneity and sampled more open conformations compared to previous, comparable experiments that studied BG505 and B41 SOSIP profiles (Fig. 2f and Ref[30]). In the presence of sCD4, 1059

SOSIP showed a transition from heterogeneous distance measurements correlated with closed and more open conformations to more dominant distance measurements that correlated with Env-sCD4 open conformations (Fig. 2f). Taken together, we conclude that the Envs of some T/F HIV-1 strains are incompletely closed.

in vivo evolution of a T/F with incompletely closed Env conformation

We studied how a T/F virus with incompletely closed Env conformation evolved post transmission in an individual infected with HIV-1_{CH040}. We selected T/F CH040 Envs because a) single genome-derived *env* sequences from the plasma were available for over >1700 days[27,42,43], b) initial analysis showed that CH040 Envs were almost completely resistant to all tested bnAbs except for VRC01 and VRC03 while maintaining high infectivity (Extended Data Figs. 3 and 11), and c) unexpectedly, entry mediated by CH040 Envs was sensitive to 19b, which targets the gp120 V3 loop, as well as to sCD4 and to cold exposure, all of which support a more open Env conformation (Fig. 3b-c and Extended Data Fig. 1). We analyzed 475 available *env* sequences (Extended Data Table 5 and Supplementary Table 2), built consensus sequences, and reconstructed *de novo* pseudoviruses displaying Envs that represent 10 different time points during CH040 Env evolution in the infected individual. Reconstructed viruses exhibited a gradual increase in resistance to 19b, cold, and sCD4 over the course of infection (Fig. 3b-c and Extended Data Fig. 12), indicating that CH040 Envs were evolving to become more closed. We detected several changes in the V3 loop during evolution but the 19b epitope in CH040 and all 41 sequenced viruses that evolved in CH040 patient by day 1737 was intact (IxxxxGxxFYxR; x=any amino acid; Supplementary Table 2). The observed evolution pattern is consistent with ability of antibodies developed in humans infected with HIV-1 to exert a selection pressure to conceal exposed Env epitopes, as well as with previous studies that monitored SHIV evolution in rhesus macaques[44,45]. It took more than 1000 days and 25 amino acid changes (Extended Data Table 5) to evolve to a more closed phenotype, which is consistent with previous observations of the development of antibodies with modest neutralization breadth in this individual[43].

With this information, we next studied how the evolution pattern from incompletely closed Env to a more closed state affected virus sensitivity to bnAbs (Fig. 3d). CH040 Envs were completely resistant to the V1/V2 loop bnAbs PG9 and PGT145 (up to 20 μg/ml) and this pattern was mostly unchanged over the course of viral evolution. Sequence analysis of CH040 Envs identified the amino acid Lys at position 160 instead of the conserved Asn, which is typically glycosylated and significantly contributes to V1/V2 bnAb sensitivity. Introduction of the Asn at position 160 rendered CH040 Envs highly sensitive to both PG9 and PGT145 (Extended Data Fig. 13). Interestingly, Lys at position 160 was not fixed during HIV-1 evolution in the infected individual but was replaced by an Arg rather than Asn during the course of evolution. Sensitivity of CH040 Envs to CD4bs VRC01 and VRC03 bnAbs was maintained over the time of infection, although the evolved virus at late time points was slightly more resistant than the T/F CH040 (Fig. 3d). The third CD4bs bnAb, 3BNC117, was ineffective against CH040 but could readily block infection of the evolved virus. Similarly, CH040 Envs were completely resistant to the V3-glycan bnAbs but became hypersensitive to these antibodies during *in vivo* evolution. We identified the E332N change in evolved viruses that typically contributes to V3-glycan bnAb sensitivity[46]. However, additional changes

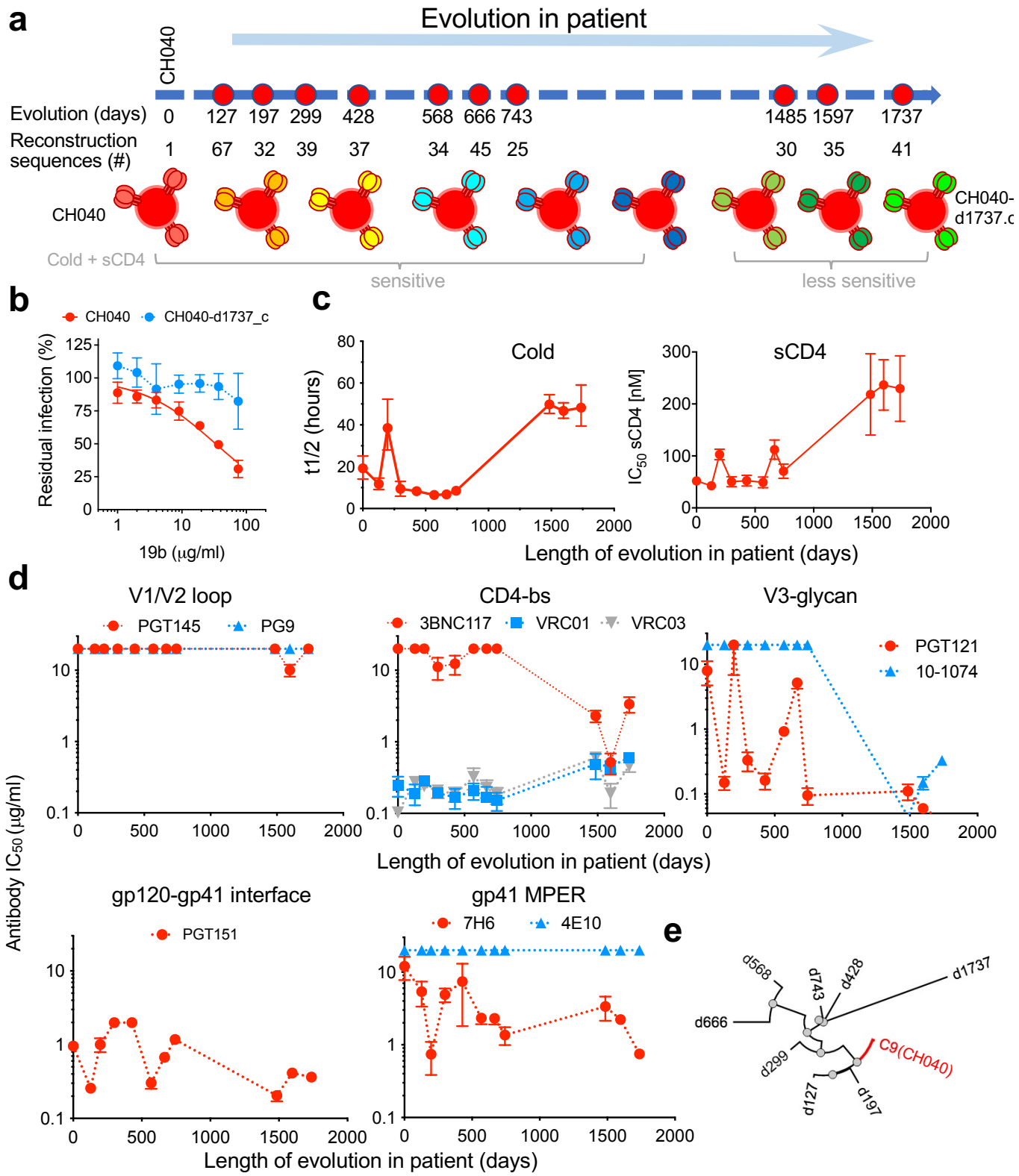

Figure 3. Reconstructing the *in vivo* evolutionary pathway of a multi-bnAb resistant T/F Envs (CH040) that partially expose the gp120 V3 loop. a, A scheme of 10 time points during evolution of CH040 Envs in infected individual in which available sequences were used to determine consensus *env* sequences and to reconstruct consensus-based pseudoviruses. **b,** Sensitivity of HIV-1 pseudotyped with T/F CH040 and CH040-d1737.c, which represents consensus of viral population that evolved by day 1737, to 19b antibody that recognizes exposed V3-loop in open Env conformation. **c,** Sensitivity of reconstructed consensus pseudoviruses to cold and sCD4. **d,** Sensitivity of reconstructed consensus pseudoviruses to bnAbs targeting different sites of Env vulnerability. **e,** Phylogenetic tree of CH040 Env evolution in the infected individual based on consensus *env* sequences (generated by NGPhylogeny.fr; Nucleic Acids Research, 47, W260–W265, 2019). Data shown are average results of at least two independent experiments, each performed in duplicate.

were required to confer sensitivity, which may include the N334S to generate the N332 related glycosylation motif Asn-X-Ser/Thr, since introducing a single E332N change into CH040 Env resulted in a virus that was still resistant to PGT121 bnAb (Extended Data Fig. 13). Sensitivity of CH040 Envs to PGT151 was maintained for at least 1737 days whereas CH040 Env sensitivity to the gp41 MPER bnAbs varied; resistance to 4E10 was maintained throughout the course of evolution but the evolved virus became more sensitive to 7H6 bnAb (Fig. 3d). Thus, *in vivo* evolution of the CH040 Envs resulted in a more closed conformation that was recognized better by a subset of bnAbs.

CD4bs bnAb breadth correlates with efficient neutralization of open and closed Env conformations

Identification of incompletely closed T/F Envs led us to hypothesize that bnAbs that can recognize multiple Env conformations exhibit broader and more potent neutralization activity. We focused on CD4bs bnAbs that typically prefer to neutralize viruses with closed Env conformations[25,36]. To evaluate the Env conformational preference during HIV-1 entry, we used the HIV-1_{JR-FL} I423A Env variant that exhibits an open conformation, based on hypersensitivity to Env ligands that recognize internal Env epitopes[25]. We compared the ability of 5 different CD4bs bnAbs: N6, 3BNC117, NIH45/46, VRC01, and VRC03 to neutralize viruses with closed (WT HIV-1_{JR-FL}) and open (HIV-1_{JR-FL} I423A) Env conformations (Fig. 4a-b). N6 exhibited a potent and specific inhibition of the closed, functional intermediate (HIV-1_{JR-FL} L193Q) and open Env conformations with only minor differences between IC_{50} values for these variants (Fig. 4a). Of note, N6 bnAb was identified by screening B cells without prior selection for binding to soluble Envs and it exhibits an ultrabroad and potent inhibition profile[31]. Consistent with an exceptional breadth, N6 efficiently neutralized diverse viruses with WT (closed) and I423A (open) Env conformations from clades A, B, C and D (Fig. 4c). In contrast, VRC01, VRC03, and 3BNC117 bnAbs preferentially neutralized viruses with closed Env conformations and exhibited a significantly reduced inhibition activity against more open Env conformations (Fig. 4b)[7,25]. To assess this phenotype in a broader context, we analyzed hundreds of HIV-1 strains in HIV database[47] and studied the relationship between CD4bs bnAb breadth (% strains inhibited with IC_{50}< 50 μg/ml), potency (expressed as geometric IC_{50}) and conformational flexibility. We detected a positive correlation between CD4bs bnAb breadth and potency, and a statistically significant correlation (P value < 0.05) between CD4bs bnAb breadth and their ability to neutralize closed, intermediate, and open Env conformations (Fig. 4d). This analysis linked exceptional breadth of N6 (ref[31]) with neutralization of multiple Env conformations. To better understand the mode of binding to and neutralization of multiple Env conformations, we solved the cryo-EM structure of 1059 SOSIP (purified by 2G12/SEC) in complex with N6 (ref[31]) and 10-1074 (ref[48]) bnAbs at 5.7 Å resolution (Fig. 4e and Extended Data Fig. 14a-d). Bound to N6 and 10-1074 bnAbs, 1059 SOSIP showed a closed Env conformation relative to the conformation observed in the structure of the 1059 SOSIP-17b complex (Figs. 4e and 2e) but moderate 5.7 Å resolution (with C3 symmetry, which was identified in the map, applied during reconstruction) precluded detailed analysis of this structure. Models of N6-gp120 (PDB IDs: 5TE4, 5TE6, and 5TE7), N6 FR3-03 scFV-SOSIP (PDB ID: 6NM6) and of other CD4bs bnAb-SOSIPs fit well to our structure (Extended Data Fig. 14e-i). To study how N6 recognizes open Env

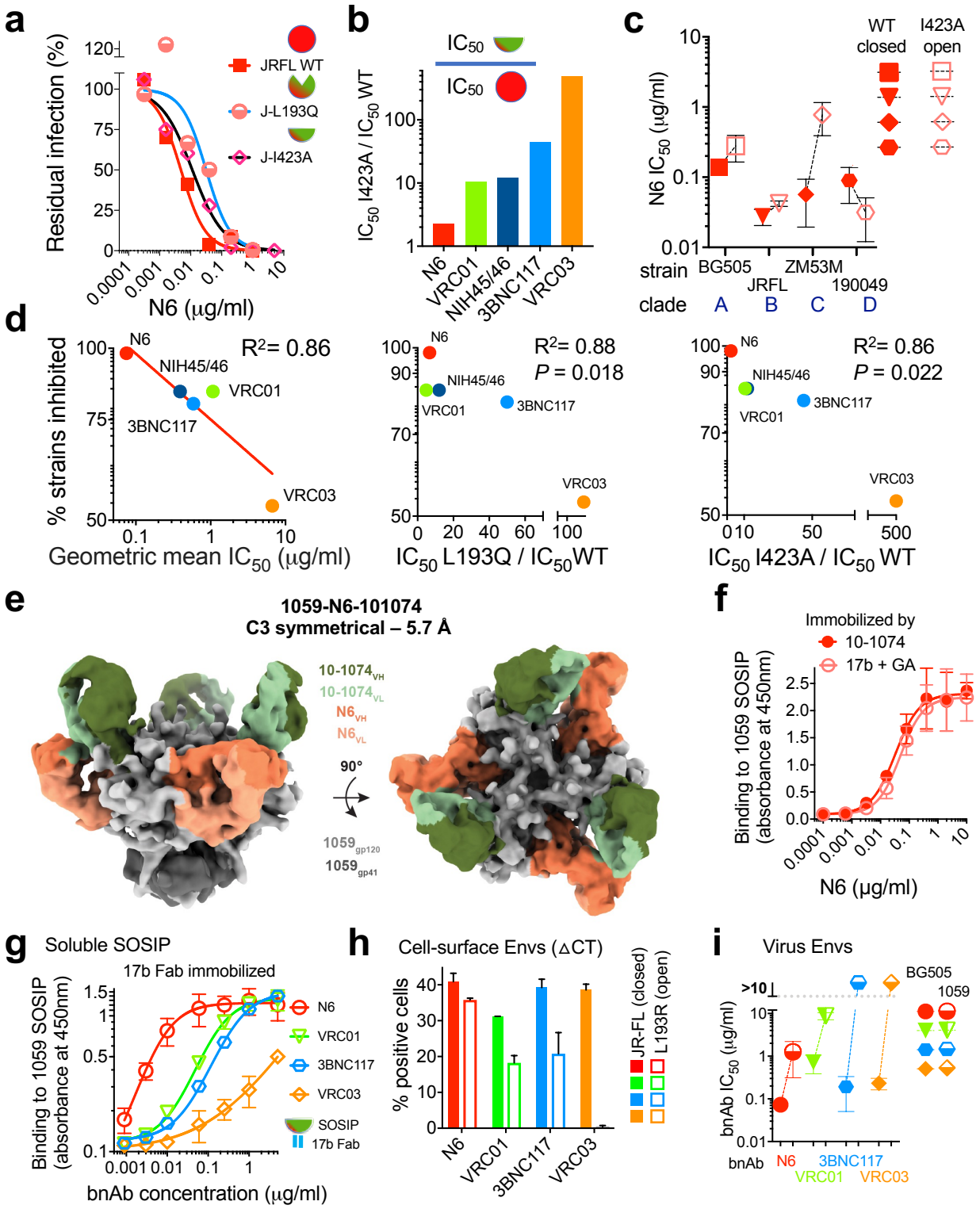

Figure 4. Relationship between neutralization of multiple Env conformations, potency and breadth of CD4bs bnAbs. **a,** Sensitivity of HIV-1 pseudotyped with WT JRFL (closed), JRFL L193Q (functional intermediate) and JRFL I423A (open) Envs to N6 bnAb. Variants were selected based on Env sensitivity to ligands recognizing open conformation (Herschhorn *et al.,* mBio 2016; Nat Commun 2017). **b,** Fold-change of neutralization sensitivity of pseudoviruses with open (JRFL I423A) and closed (JRFL WT) Env conformations to different CD4bs bnAbs. **c,** Sensitivity of HIV-1 pseudotyped with the closed (WT) and open (I423A) Env conformations of strains from diverse clades to N6. **d,** Relationship between the breadth of CD4bs bnAbs and their potency (left), bnAb breadth and efficiency to neutralize HIV-1_{JRFL} Env functional intermediate (center), and bnAb breadth and efficiency to neutralize HIV-1_{JRFL} Env open conformation (right). See also Extended Data Fig. 15. **e,** Cryo-EM structure of 1059 SOSIP in complex with N6 and 10-1074 bnAbs. **f-g**, ELISA of N6 (**f**) or CD4bs bnAbs (**g**) binding to 1059 SOSIP immobilized via 17b IgG or Fab to stabilize open Env conformation. **h**, Flow cytometric analysis of bnAb binding to cell-surface closed and open JR-FL Envs. ΔCT, cytoplasmic tail deleted. **i**, Sensitivity of BG505 and 1059 pseudoviruses to CD4bs bnAbs.

conformations, we measured N6 binding to 1059 SOSIP that was immobilized by 17b, which stabilizes the open Env conformation. N6 binding to 17b-immobilized 1059 SOSIP was comparable to N6 binding to 1059 SOSIP that was immobilized by the control 2G12 antibody, which exhibits no conformational preference, and to N6 binding to 1059 SOSIP immobilized by 10-1074, for which we solved the structure at moderate 5.7 Å resolution (Fig. 4f and Extended Data Fig. 15b). N6 also bound glutaraldehyde-crosslinked 1059 SOSIP as efficiently as non-crosslinked 1059 SOSIP (Extended Data Fig. 15b). Notably, N6 recognized open 1059 SOSIP Envs and open Envs expressed on the cell surface more efficiently than VRC01, 3BNC117, and VRC03 (Fig. 4g-h). Consistent with strong binding of different Env conformations and in contrast to VRC01, 3BNC117 and VRC03 bnAbs, N6 efficiently neutralized HIV-1 with tightly closed (BG505) and incompletely closed (1059) Envs (Fig. 4i).

Resistance of 1059 Envs to most CD4bs bnAbs highlights one potential mechanism by which incompletely closed Env conformation can escape bnAb neutralization. In this context, we analyzed the HIV-1 Envs from the recent first-in-humans antibody-mediated prevention (AMP; HVTN 704) trial, in which the CD4bs bnAb VRC01 was administered to healthy individuals at risk as a potential prevention modality[49]. VRC01-resistant Envs were isolated from VRC01-treated individuals who acquired HIV-1 despite the presence of VRC01, and also from individuals in the placebo arm. We tested the sensitivity of Envs isolated in this trial to ligands and cold and detected a statistically significant correlation between resistance to VRC01 and hypersensitivity to cold (P=0.001), which is associated with more open Env conformations (Fig. 5a-b). Moreover, some VRC01-resistant Envs were susceptible to specific internal-epitope antibodies such as 39F (binds gp120 V3), E51 (binds gp120 CCR5-bs), and 246-D (binds gp41) in comparison with VRC01-sensitive Envs although, as expected, not every exposure of internal epitopes resulted in VRC01 resistance (Fig. 5c-d, and Extended Data Fig. 16). Principal component analysis of Env sensitivity clustered VRC01 sensitivity opposite to E51, 17b, 246-D and cold sensitivities (Fig. 5d). Of note, 1059 is resistant to VRC01 and exhibited similar hypersensitivity to cold, and to E51 antibody (Extended Data Figs. 1 and 2). With one exception (of a single VRC03-sensitive strain), all VRC01-resistant Envs were also resistant to VRC03 and 3BNC117 (IC_{50} > 5μg/ml) that, similarly to VRC01, prefer to neutralize the closed Env conformation (Fig. 5e)[7,25]. Despite resistance to VRC01, gp120 of most resistant AMP Envs bound VRC01 (based on enzyme-linked immunosorbent assay) at concentrations that exhibit no significant effect on viral entry of these resistant strains (Fig. 5e-g), suggesting interference with VRC01 access to its epitope on the native HIV-1 Envs on virions. In contrast to VRC01, VRC03 and 3BNC117, the ultra-broad N6 bnAb, which neutralizes both closed and open Env conformations, blocked the entry of 50% of the VRC01-resistant strains at IC_{50} < 1.2 μg/ml (Fig. 5e). All VRC01-sensitive Envs were sensitive to all other CD4bs bnAbs tested except for one specific Envs that was resistant to VRC03 (Fig. 5e). Overall, these observations suggest that N6 directly binds open, intermediate, incompletely closed, and closed Env conformations, and this ability allows N6 to potently neutralize diverse Env conformations that exist in different primary HIV-1 strains. Env conformational flexibility may allow some HIV-1 strains to escape CD4bs bnAbs that preferentially neutralize the tightly-closed Env conformation (e.g. VRC01).

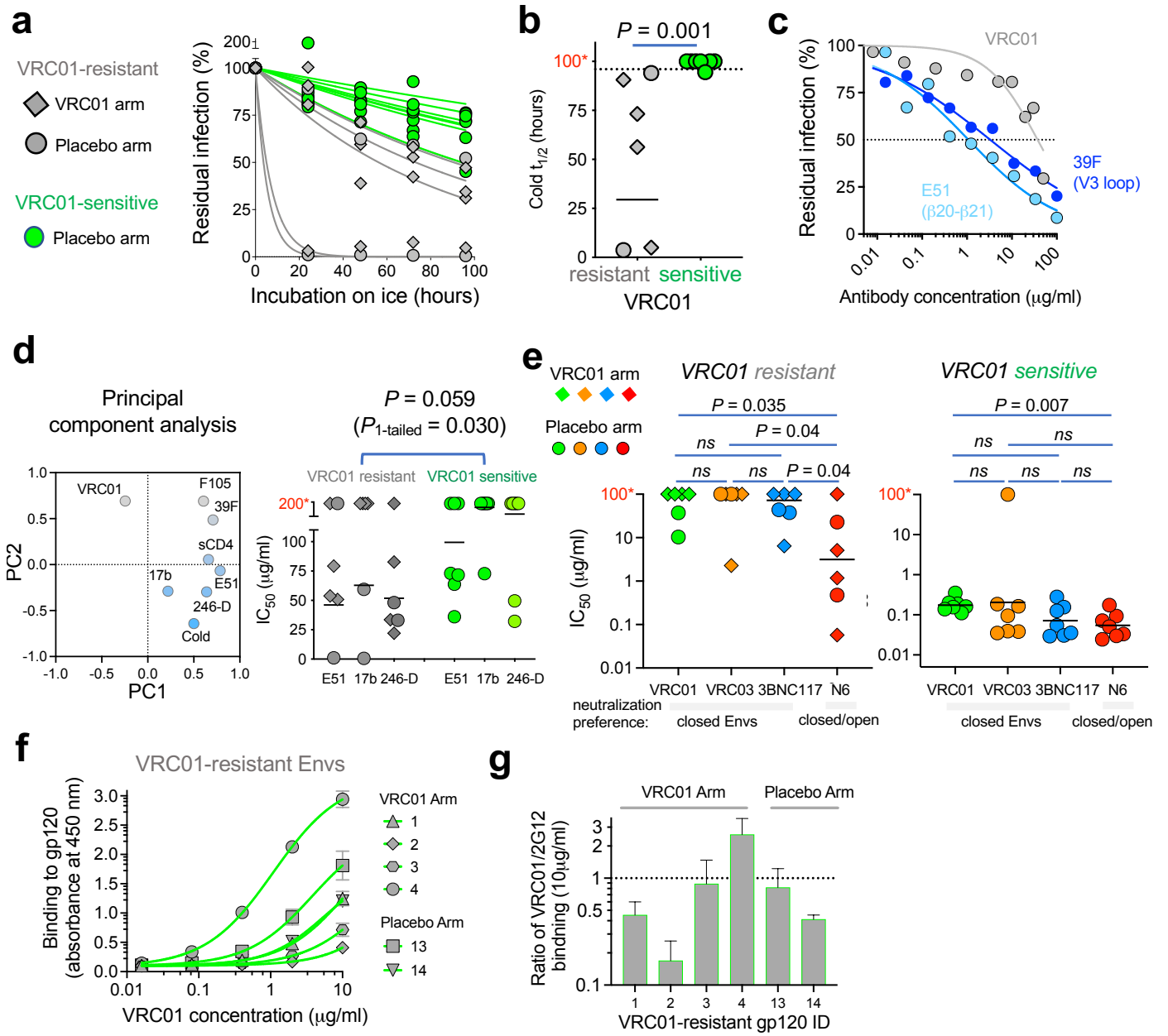

Figure 5. Analysis of HIV-1 Envs isolated from the first-in-humans antibody (VRC01) mediated prevention (AMP) trial (HVTN 704). **a,** Sensitivity to cold exposure of VRC01-resistant Envs, isolated from the VRC01 or placebo arms, and of VRC01-sensitive Envs, isolated from the placebo arm. **b,** Statistical analysis of difference between cold sensitivity of VRC01-resistant and VRC01-sensitive Envs. Half life on ice was calculated by fitting zero-order decay curves to the residual infection data (panel **a**). A dot line represents the maximal experimental time (96 hours) tested. **c,** Sensitivity of Envs from a single VRC01-resistant strain (H704_1835_150_RE_p002s_2484A) to VRC01 and to internal-epitope antibodies that target different gp120 domains. **d,** Left - principal component analysis (PCA) of AMP Envs (6 VRC01-resistant & 7 VRC01-sensitive) clustered VRC01 sensitivity opposite to E51, 17b, 246-D and cold sensitivities. All Envs were resistant to 19b and 697-30D and thus these antibodies were not included. Right - statistical analysis of the difference between the sensitivity of VRC01-resistant and VRC01-sensitive Envs to 3 Abs (E51, 17b, and 246-D) identified by PCA. IC_{50s} were calculated from dose-response curves (Extended Data Fig. 16). No differences were identified for all other Env ligands or for comparison of VRC01-resistant and VRC01-sensitive for each antibody separately (Extended Data Fig. 16). **e,** Sensitivity of VRC01-resistant (left) and VRC01-sensitive (right) Envs to CD4bs bnAbs. **f,** Binding of VRC01 to soluble AMP gp120s by ELISA. **g,** 2G12-nornalized VRC01 binding to AMP gp120s. $t_{1/2}$ values or IC_{50s} higher than the maximal concentration/time tested (96 hours (**b**), 100 μg/ml (**d**) and 50 μg/ml (**e**)) were set to an arbitrary 100 hours (**b**), 200 μg/ml (**d**) and 100 μg/ml concentrations (**e**), which are labeled with red letters and an asterisk on the Y-axis. *P,* two-tailed *P* value of Mann-Whitney U-test. ns, not significant. Results are the average of 2-5 independent experiments, each performed in duplicate.

Conclusions

Here we present evidence that the functional Envs of some T/F HIV-1 strains sample incompletely closed conformations. Six out of thirteen T/F strains exhibited partial exposure of internal Env epitopes that was apparently compatible with HIV-1 transmission. We selected highly infectious T/F Envs to ensure robust and reproducible results; the levels of viral infectivity were unrelated to internal-epitope exposure, sCD4 or cold sensitivity (Extended Data Fig. 2e), and thus our approach likely recapitulates a general phenotype of Env function. Our results (6/13; 46%) may underestimate the true number of incompletely closed Envs as our ability to identify this phenotype is limited by available antibodies and the presence of their epitopes in all strains. Consistent with this understanding, incompletely closed T/F Envs were hypersensitive to cold, which is an antibody-independent method associated with more open Env conformations[7,18,34]. The 17b and E51 antibodies bind to epitopes that overlap with the coreceptor-bs and contact the β20-β21 element of gp120, which regulates Env transitions between different conformations[25,50]. Changes in two Env resides, K421 and Q422, which are main 17b and E51 contacts and typically are not exposed in primary isolates, lead to opening of the Env trimer and hypersensitivity to Env ligands that recognize internal epitopes[25]. Thus, weak-moderate recognition of 1059, SC45 and WEAU Env trimers expressed on the surface of HIV-1 by 17b and E51 (Extended Data Fig. 1), and 17b accessibility to these residues on soluble 1059 SOSIP (Extended Data Figs. 5 and 8) suggest that the β20-β21 regulatory switch in some incompletely closed Envs is oriented in favorable downstream configuration. Cryo-EM structure of the unliganded 1059 SOSIP provides new insights into an incompletely closed Envs. Asymmetry, increased conformational flexibility and scissoring motions provide the first long-sought structural evidence for putative “breathing” ability of HIV-1 Envs. Our experimental finding is consistent with previous molecular dynamics simulations of a fully glycosylated unliganded HIV-1 BG505 SOSIP Env trimer, in which protomer flexing about the trimer axis (i.e. scissoring motion) coupled with steric occlusion by glycans was found to restrict access to the CD4bs[51] and with studies that associated trimer asymmetry with initial response to CD4[52,53]. V1/V2 movement such as the one induced by amino acid changes in V1/V2 (e.g. L193A) can lead to HIV-1 resistance to VRC01, VRC03, and 3BNC117 bnAbs[7,18,25], similar to the resistance profile that we measured for 1059 (Extended Data Fig. 3). Of note, 1059 Envs provide the highest (22.6%) T cell epitope (9-mer) coverage among T/F Envs and has been tested as a preferred Env immunogen in non-human primates[54] and more recently in humans (HVTN 106; NCT02296541). Thus, amino acid sequence of 1059 Envs that determines an incompletely-closed conformation also contains many common T cell epitopes.

Post transmission evolution of the incompletely closed CH040 T/F Envs towards more closed conformation is consistent with the known pressure of strain-specific neutralizing antibodies that are developed in individuals infected with HIV-1. We hypothesize that generation of incompletely closed Envs potentially increases the number of alternative pathways to adapt to a closed Env conformation in comparison with maintaining the closed Env conformation at all times, which is expected to limit the allowed changes and possible pathways to escape neutralizing antibodies. Additionally, temporal existence of more open Env conformations may facilitate the infection of cells that express low levels of CD4[7,25] and Env interactions with CD4 receptors of additional

species[55].

Our results suggest that incompletely closed Envs are a heterogeneous collection of similar but not identical Env conformations. The gp120 V3 region is the first and most common element to be exposed on the Envs of T/F isolates and of intermediate variants generated *in vitro*, consistent with previous reports of V3 metastability[20,56]. We found that alternative and multiple routes for Envs to exist in incompletely closed conformations can potentially affect bnAb sensitivity in different ways. For example, CH040 Envs expose the V3 loop according to 19b sensitivity and are resistant to V3-glycan PGT121 and 10-1074 bnAbs (Fig. 3); 1059 Envs partially expose the coreceptor-bs as indicated by moderate 17b and E51 sensitivities and are resistant to several CD4bs and V1/V2 loop bnAbs (Extended Data Figs. 1 and 3). In contrast, WEAU Envs are sensitive to different antibodies that target internal epitopes as well as to most bnAbs tested (Fig. 1 and Extended Data Figs. 1 and 3). Thus, strain-specific heterogeneity of the incompletely close Env conformations may affect bnAb sensitivity.

HIV-1 Env resistance to multiple CD4bs bnAbs among VRC01-resistant strains from the AMP trial highlights a potential mechanism by which incompletely closed Env conformation can escape neutralization by several bnAbs. These results underlie potential pathways of global HIV-1 resistance to VRC01-like bnAbs and highlight to superiority of CD4bs bnAbs that neutralize multiple Env conformations. Thus, bnAbs recognizing diverse Env conformations may have superior breadth and some V3-glycan bnAbs neutralize different Env conformations because they recognize conserved glycans that are unaffected by Env transitions. Similarly, the gp120-gp41 interface bnAb 8ANC195 recognizes partially open and closed conformations and prevents full opening of Env trimer by binding to protein residues and three N-linked glycans attached to Asn234, Asn276, and Asn637 (ref[57]). However, the breadth of these bnAbs against diverse HIV1- strains is limited by heterogeneous glycosylation patterns in cells. In contrast, recognition of highly conserved amino acids and open Env conformations by MPER and N6 bnAbs are associated with ultra-broad neutralization. Thus, affinity maturation of N6 optimized Env binding to a maximum number of highly conserved amino acid residues, all or most of which are accessible on both the open and closed Env conformations; this strategy allows N6 to neutralize 98% of HIV-1 isolates[31]. Our previous studies and current results highlight potential consequences of Env partial opening to HIV-1 resistance to bnAbs that prefer to neutralize the closed Env conformation. Our data suggest that there are many alternative pathways by which HIV-1 Envs can become incompletely closed or even partially open and only some of these alternatives will lead to bnAb resistance. Importantly, while VRC01, VRC03 and 3BNC117 bnAbs are still mostly effective against Envs of lab-adapted HIV-1 strains that evolved *in vitro* to become fully open, N6 is effective against these strains and, in addition, primary HIV-1 Envs that are stabilized in more open states (e.g., JRFL L193Q). Thus, additional constraints are imposed to restrict opening of Envs of primary strains compared with opening of lab-adapted Envs, which may be fully accessible to antibodies. N6 will likely be more effective than VRC01, VRC03, and 3BNC117 against primary Envs as they evolve to incompletely closed conformations (e.g., 1059). Two additional broad and potent CD4bs bnAbs, Ab1-18 and N49P7, have been recently identified[58,59] and may have a similar mode of action.

Our study has several limitations. We tested a relatively small number of Envs from two separate and independent panels (T/F and AMP Envs) and, thus, our observations may not accurately represent the proportion of incompletely closed Envs in the viral population. Our mechanistic insights are based on structure of SOSIP Env and may have underestimated Env opening as this soluble format was originally engineered to capture closed, prefusion Env conformation. We analyzed symmetry of only two SOSIPs purified via *Galanthus nivalis* lectin under identical conditions; we expect that analysis of SOSIP Envs of additional HIV-1 strains, which are planned for future studies, will reveal a range of asymmetries that may relate to the ability of different Envs to "breathe". Despite these limitations, our results clearly refine the current knowledge of HIV-1 conformation heterogeneity and provide evidence that not every HIV-1 Env from ~37 million different individuals infected with HIV-1 adopts a single identical closed Env conformation. Maintenance of a closed Env conformation is balanced by Env conformational flexibility within the circulating HIV-1 population and during Env synthesis and evolution in patients. The existence of incompletely closed Env conformation impacts the development of next generation bnAbs for immunotherapy, the design of Env immunogens and the understanding of HIV-1 Env function and inhibition. Our results, together with the outcome of several clinical trials[49,60,61], suggest prioritizing N6-like bnAbs as preferred candidates for future trials using CD4bs bnAbs. Moreover, recent success in immunogen-based priming of germline precursors for anti-CD4bs bnAb development[62] may benefit from subsequent shepherding antibody development toward N6-like bnAbs. In parallel, an alternative vaccine approach in which a combination of tightly- and incompletely-closed Env immunogens are presented to the immune system may be an efficient way to mount a broad antibody response against diverse HIV-1 strains, some of which display incompletely closed Envs. In this context, the HVTN 106 trial (NCT02296541) has tested the immune response of DNA-based 1059 Env immunogen in humans with the aim of induction both efficient B and T cell Env responses and upcoming results will further inform the development of new approaches using incompletely-closed Env immunogens.

References

1. Allan, J. S. *et al.* Major glycoprotein antigens that induce antibodies in AIDS patients are encoded by HTLV-III. *Science* **228**, 1091–4 (1985).
2. Wyatt, R. *et al.* The antigenic structure of the HIV gp120 envelope glycoprotein. *Nature* **393**, 705–11 (1998).
3. Choe, H. *et al.* The beta-chemokine receptors CCR3 and CCR5 facilitate infection by primary HIV-1 isolates. *Cell* **85**, 1135–48 (1996).
4. Feng, Y., Broder, C. C., Kennedy, P. E. & Berger, E. A. HIV-1 entry cofactor: functional cDNA cloning of a seven-transmembrane, G protein-coupled receptor. *Science* **272**, 872–7 (1996).
5. Dragic, T. *et al.* HIV-1 entry into CD4+ cells is mediated by the chemokine receptor CC-CKR-5. *Nature* **381**, 667–73 (1996).
6. Liu, J., Bartesaghi, A., Borgnia, M. J., Sapiro, G. & Subramaniam, S. Molecular architecture of native HIV-1 gp120 trimers. *Nature* **455**, 109–13 (2008).
7. Herschhorn, A. *et al.* Release of gp120 restraints leads to an entry-competent intermediate state of the HIV-1 envelope glycoproteins. *mBio* **7**, 1–12 (2016).
8. Wu, L. *et al.* CD4-induced interaction of primary HIV-1 gp120 glycoproteins with the chemokine receptor

CCR-5. *Nature* **384**, 179–83 (1996).
9. Trkola, A. *et al.* CD4-dependent, antibody-sensitive interactions between HIV-1 and its co-receptor CCR-5. *Nature* **384**, 184–7 (1996).
10. Furuta, R. A., Wild, C. T., Weng, Y. & Weiss, C. D. Capture of an early fusion-active conformation of HIV-1 gp41. *Nat. Struct. Biol.* **5**, 276–9 (1998).
11. He, Y. *et al.* Peptides trap the human immunodeficiency virus type 1 envelope glycoprotein fusion intermediate at two sites. *J. Virol.* **77**, 1666–71 (2003).
12. Koshiba, T. & Chan, D. C. The prefusogenic intermediate of HIV-1 gp41 contains exposed C-peptide regions. *J. Biol. Chem.* **278**, 7573–9 (2003).
13. Yang, Z., Wang, H., Liu, A. Z., Gristick, H. B. & Bjorkman, P. J. Asymmetric opening of HIV-1 Env bound to CD4 and a coreceptor-mimicking antibody. *Nat. Struct. Mol. Biol.* **26**, 1167–1175 (2019).
14. Ladinsky, M. S. *et al.* Electron tomography visualization of HIV-1 fusion with target cells using fusion inhibitors to trap the pre-hairpin intermediate. *eLife* **9**, 1–18 (2020).
15. Jette, C. A. *et al.* Cryo-EM structures of HIV-1 trimer bound to CD4-mimetics BNM-III-170 and M48U1 adopt a CD4-bound open conformation. *Nat. Commun.* **12**, 1–10 (2021).
16. Kong, R. *et al.* Fusion peptide of HIV-1 as a site of vulnerability to neutralizing antibody. *Science* **352**, 828–33 (2016).
17. Ozorowski, G. *et al.* Open and closed structures reveal allostery and pliability in the HIV-1 envelope spike. *Nature* **547**, 360–361 (2017).
18. Herschhorn, A. *et al.* A broad HIV-1 inhibitor blocks envelope glycoprotein transitions critical for entry. *Nat. Chem. Biol.* **10**, 845–852 (2014).
19. Si, Z. *et al.* Small-molecule inhibitors of HIV-1 entry block receptor-induced conformational changes in the viral envelope glycoproteins. *Proc. Natl. Acad. Sci. U. S. A.* **101**, 5036–41 (2004).
20. Ivan, B., Sun, Z., Subbaraman, H., Friedrich, N. & Trkola, A. CD4 occupancy triggers sequential pre-fusion conformational states of the HIV-1 envelope trimer with relevance for broadly neutralizing antibody activity. *PLOS Biol.* **17**, e3000114 (2019).
21. Weissenhorn, W., Dessen, A., Harrison, S. C., Skehel, J. J. & Wiley, D. C. Atomic structure of the ectodomain from HIV-1 gp41. *Nature* **387**, 426–430 (1997).
22. Lu, M., Blacklow, S. C. & Kim, P. S. A trimeric structural domain of the HIV-1 transmembrane glycoprotein. *Nat. Struct. Biol.* **2**, 1075–82 (1995).
23. Tan, K., Liu, J., Wang, J., Shen, S. & Lu, M. Atomic structure of a thermostable subdomain of HIV-1 gp41. *Proc. Natl. Acad. Sci. U. S. A.* **94**, 12303–8 (1997).
24. Melikyan, G. B. *et al.* Evidence that the transition of HIV-1 gp41 into a six-helix bundle, not the bundle configuration, induces membrane fusion. *J. Cell Biol.* **151**, 413–23 (2000).
25. Herschhorn, A. *et al.* The β20-β21 of gp120 is a regulatory switch for HIV-1 Env conformational transitions. *Nat. Commun.* **8**, 1049 (2017).
26. Han, Q. *et al.* Difficult-to-neutralize global HIV-1 isolates are neutralized by antibodies targeting open envelope conformations. *Nat. Commun.* **10**, (2019).
27. Keele, B. F. *et al.* Identification and characterization of transmitted and early founder virus envelopes in primary HIV-1 infection. *Proc. Natl. Acad. Sci. U. S. A.* **105**, 7552–7557 (2008).
28. Boliar, S. *et al.* Ligand accessibility to the HIV-1 Env co-receptor binding site can occur prior to CD4 engagement and is independent of viral tier category. *Virology* **519**, 99–105 (2018).
29. Sullivan, N. *et al.* CD4-Induced Conformational Changes in the Human Immunodeficiency Virus Type 1 gp120 Glycoprotein: Consequences for Virus Entry and Neutralization. *J. Virol.* **72**, 4694–4703 (1998).
30. Stadtmueller, B. M. *et al.* DEER Spectroscopy Measurements Reveal Multiple Conformations of HIV-1 SOSIP Envelopes that Show Similarities with Envelopes on Native Virions. *Immunity* **49**, 235-246.e4 (2018).
31. Huang, J. *et al.* Identification of a CD4-Binding-Site Antibody to HIV that Evolved Near-Pan Neutralization Breadth. *Immunity* **45**, 1108–1121 (2016).
32. Parrish, N. F. *et al.* Phenotypic properties of transmitted founder HIV-1. *Proc. Natl. Acad. Sci.* **110**, 6626–6633 (2013).
33. Foster, T. L. *et al.* Resistance of Transmitted Founder HIV-1 to IFITM-Mediated Restriction. *Cell Host*

Microbe **20**, 429–442 (2016).
34. Kassa, A. *et al.* Transitions to and from the CD4-bound conformation are modulated by a single-residue change in the human immunodeficiency virus type 1 gp120 inner domain. *J. Virol.* **83**, 8364–78 (2009).
35. Rathinakumar, R., Dutta, M., Zhu, P., Johnson, W. E. & Roux, K. H. Binding of anti-membrane-proximal gp41 monoclonal antibodies to CD4-liganded and -unliganded human immunodeficiency virus type 1 and simian immunodeficiency virus virions. *J. Virol.* **86**, 1820–31 (2012).
36. Flemming, J., Wiesen, L. & Herschhorn, A. Conformation-Dependent Interactions Between HIV-1 Envelope Glycoproteins and Broadly Neutralizing Antibodies. *AIDS Res. Hum. Retroviruses* **34**, 794–803 (2018).
37. Harris, A. K., Bartesaghi, A., Milne, J. L. S. & Subramaniam, S. HIV-1 envelope glycoprotein trimers display open quaternary conformation when bound to the gp41 membrane-proximal external-region-directed broadly neutralizing antibody Z13e1. *J. Virol.* **87**, 7191–6 (2013).
38. HIV Databases. https://www.hiv.lanl.gov/content/index.
39. Hubbell, W. L., López, C. J., Altenbach, C. & Yang, Z. Technological advances in site-directed spin labeling of proteins. *Curr. Opin. Struct. Biol.* **23**, 725–733 (2013).
40. Hubbell, WL., Cafiso, DS. & Altenbach, C. Identifying conformational changes with site-directed spin labeling. *Nat. Struct. Biol.* **7**, 735–739 (2000).
41. Jeschke, G. DEER distance measurements on proteins. *Annu. Rev. Phys. Chem.* **63**, 419–446 (2012).
42. Bar, K. J. *et al.* Early low-titer neutralizing antibodies impede HIV-1 replication and select for virus escape. *PLoS Pathog.* **8**, (2012).
43. Wagh, K. *et al.* Completeness of HIV-1 Envelope Glycan Shield at Transmission Determines Neutralization Breadth. *Cell Rep.* **25**, 893-908.e7 (2018).
44. McGee, K. *et al.* The selection of low envelope glycoprotein reactivity to soluble CD4 and cold during simian-human immunodeficiency virus infection of rhesus macaques. *J. Virol.* **88**, 21–40 (2014).
45. Moody, M. A. *et al.* Strain-Specific V3 and CD4 Binding Site Autologous HIV-1 Neutralizing Antibodies Select Neutralization-Resistant Viruses. *Cell Host Microbe* **18**, 354–362 (2015).
46. Walker, L. M. *et al.* Broad neutralization coverage of HIV by multiple highly potent antibodies. *Nature* **477**, 466–470 (2011).
47. Yoon, H. *et al.* CATNAP: a tool to compile, analyze and tally neutralizing antibody panels. *Nucleic Acids Res.* **43**, W213–W219 (2015).
48. Mouquet, H. *et al.* Complex-type N-glycan recognition by potent broadly neutralizing HIV antibodies. *Proc. Natl. Acad. Sci. U. S. A.* **109**, (2012).
49. Corey, L. *et al.* Two Randomized Trials of Neutralizing Antibodies to Prevent HIV-1 Acquisition. *N. Engl. J. Med.* **384**, 1003–1014 (2021).
50. Rizzuto, C. D. *et al.* A conserved HIV gp120 glycoprotein structure involved in chemokine receptor binding. *Science* **280**, 1949–1953 (1998).
51. Lemmin, T., Soto, C., Stuckey, J. & Kwong, P. D. Microsecond Dynamics and Network Analysis of the HIV-1 SOSIP Env Trimer Reveal Collective Behavior and Conserved Microdomains of the Glycan Shield. *Struct. Lond. Engl. 1993* **25**, 1631-1639.e2 (2017).
52. Li, W. *et al.* Asymmetric HIV-1 envelope trimers bound to one and two CD4 molecules are intermediates during membrane binding. 2022.12.23.521843 Preprint at https://doi.org/10.1101/2022.12.23.521843 (2022).
53. Liu, Q. *et al.* Quaternary contact in the initial interaction of CD4 with the HIV-1 envelope trimer. *Nat. Struct. Mol. Biol.* **24**, 370–378 (2017).
54. SL, H. *et al.* Comparison of Immunogenicity in Rhesus Macaques of Transmitted-Founder, HIV-1 Group M Consensus, and Trivalent Mosaic Envelope Vaccines Formulated as a DNA Prime, NYVAC, and Envelope Protein Boost. *J. Virol.* **89**, 6462–6480 (2015).
55. Vilmen, G. *et al.* Conformation of HIV-1 Envelope Governs Rhesus CD4 Usage and Simian-Human Immunodeficiency Virus Replication. *mBio* **13**, e0275221 (2022).
56. Zolla-Pazner, S. *et al.* Structure/Function Studies Involving the V3 Region of the HIV-1 Envelope Delineate Multiple Factors That Affect Neutralization Sensitivity. *J. Virol.* **90**, 636–649 (2016).
57. Scharf, L. *et al.* Broadly Neutralizing Antibody 8ANC195 Recognizes Closed and Open States of HIV-1

Env. *Cell* **162**, 1379–1390 (2015).
58. Sajadi, M. M. *et al.* Identification of Near-Pan-neutralizing Antibodies against HIV-1 by Deconvolution of Plasma Humoral Responses. *Cell* **173**, 1783-1795.e14 (2018).
59. Schommers, P. *et al.* Restriction of HIV-1 Escape by a Highly Broad and Potent Neutralizing Antibody. *Cell* **180**, 471-489.e22 (2020).
60. Herschhorn, A. Indirect Mechanisms of HIV-1 Evasion from Broadly Neutralizing Antibodies In Vivo. *ACS Infect. Dis.* (2022) doi:10.1021/acsinfecdis.2c00573.
61. Bar, K. J. *et al.* Effect of HIV Antibody VRC01 on Viral Rebound after Treatment Interruption. *N. Engl. J. Med.* **375**, 2037–2050 (2016).
62. Leggat, D. J. *et al.* Vaccination induces HIV broadly neutralizing antibody precursors in humans. *Science* **378**, eadd6502 (2022).
63. Ratnapriya, S., Chov, A. & Herschhorn, A. A Protocol for Studying HIV-1 Envelope Glycoprotein Function. *STAR Protoc.* **1**, 100133 (2020).
64. Harris, M. *et al.* Slow Receptor Binding of the Noncytopathic HIV-2UC1 Envs Is Balanced by Long-Lived Activation State and Efficient Fusion Activity. *Cell Rep.* **31**, 107749 (2020).
65. Herschhorn, A. & Hizi, A. Virtual screening, identification, and biochemical characterization of novel inhibitors of the reverse transcriptase of human immunodeficiency virus type-1. *J. Med. Chem.* **51**, 5702–5713 (2008).
66. Cervera, H., Ratnapriya, S., Chov, A. & Herschhorn, A. Changes in the V1 Loop of HIV-1 Envelope Glycoproteins Can Allosterically Modulate the Trimer Association Domain and Reduce PGT145 Sensitivity. *ACS Infect. Dis.* **7**, 1558–1568 (2021).
67. Weitman, M. *et al.* Structure-activity relationship studies of 1-(4-chloro-2,5-dimethoxyphenyl) -3-(3-propoxypropyl)thiourea, a non-nucleoside reverse transcriptase inhibitor of human immunodeficiency virus type-1. *Eur. J. Med. Chem.* **46**, 447–467 (2011).
68. Herschhorn, A., Oz-Gleenberg, I. & Hizi, A. Mechanism of inhibition of HIV-1 reverse transcriptase by the novel broad-range DNA polymerase inhibitor N-{2-[4-(Aminosulfonyl)phenyl]ethyl}-2-(2-thienyl)acetamide. *Biochemistry* **47**, (2008).
69. Ratnapriya, S. *et al.* Intra- and extra-cellular environments contribute to the fate of HIV-1 infection. *Cell Rep.* **36**, (2021).
70. Herschhorn, A. *et al.* An inducible Cell-Cell fusion system with integrated ability to measure the efficiency and specificity of HIV-1 entry inhibitors. *PLoS ONE* **6**, (2011).
71. Herschhorn, A., Marasco, W. a & Hizi, A. Antibodies and lentiviruses that specifically recognize a T cell epitope derived from HIV-1 Nef protein and presented by HLA-C. *J. Immunol.* **185**, 7623–32 (2010).
72. Cupo, A. *et al.* Optimizing the production and affinity purification of HIV-1 envelope glycoprotein SOSIP trimers from transiently transfected CHO cells. *PloS One* **14**, e0215106 (2019).
73. Sanders, R. W. *et al.* A Next-Generation Cleaved, Soluble HIV-1 Env Trimer, BG505 SOSIP.664 gp140, Expresses Multiple Epitopes for Broadly Neutralizing but Not Non-Neutralizing Antibodies. *PLoS Pathog.* **9**, e1003618 (2013).
74. Pugach, P. *et al.* A native-like SOSIP.664 trimer based on an HIV-1 subtype B env gene. *J. Virol.* **89**, 3380–3395 (2015).
75. Punjani, A., Rubinstein, J. L., Fleet, D. J. & Brubaker, M. A. CryoSPARC: Algorithms for rapid unsupervised cryo-EM structure determination. *Nat. Methods* **14**, 290–296 (2017).
76. Warshaviak, D. T., Khramtsov, V. V., Cascio, D., Altenbach, C. & Hubbell, W. L. Structure and dynamics of an imidazoline nitroxide side chain with strongly hindered internal motion in proteins. *J. Magn. Reson.* **232**, 53–61 (2013).
77. Rohou, A. & Grigorieff, N. CTFFIND4: Fast and accurate defocus estimation from electron micrographs. *J. Struct. Biol.* **192**, 216–221 (2015).
78. Adams, P. D. *et al.* PHENIX: a comprehensive Python-based system for macromolecular structure solution. *Acta Crystallogr. D Biol. Crystallogr.* **66**, 213–221 (2010).
79. Scheres, S. RELION: implementation of a Bayesian approach to cryo-EM structure determination. *J. Struct. Biol.* **180**, 519–530 (2012).
80. Zheng, S. Q. *et al.* MotionCor2: Anisotropic correction of beam-induced motion for improved cryo-electron

microscopy. *Nat. Methods* **14**, 331–332 (2017).
81. Tan, Y. *et al.* Addressing preferred specimen orientation in single-particle cryo-EM through tilting. *Nat. Methods* **14**, 793–796 (2017).
82. Webb, B. & Sali, A. Comparative Protein Structure Modeling Using MODELLER. *Curr. Protoc. Bioinforma.* **54**, 5.6.1-5.6.37 (2016).
83. Emsley, P., Lohkamp, B., Scott, W. G. & Cowtan, K. Features and development of Coot. *Acta Crystallogr. D Biol. Crystallogr.* **66**, 486–501 (2010).
84. Croll, T. I. ISOLDE: a physically realistic environment for model building into low-resolution electron-density maps. *Acta Crystallogr. Sect. Struct. Biol.* **74**, 519–530 (2018).
85. Punjani, A. & Fleet, D. J. 3D variability analysis: Resolving continuous flexibility and discrete heterogeneity from single particle cryo-EM. *J. Struct. Biol.* **213**, 107702 (2021).
86. Goddard, T. *et al.* UCSF ChimeraX: Meeting modern challenges in visualization and analysis. *Protein Sci. Publ. Protein Soc.* **27**, 14–25 (2018).

Acknowledgments

We thank B.H. Hahn (University of Pennsylvania), G.M. Shaw (University of Pennsylvania), and K. Wagh (Los Alamos National Laboratory) for reading the manuscript and providing critical comments. We thank the NIH AIDS Reagent Program, Division of AIDS, NIAID, NIH for providing the following anti-HIV-1 Env antibodies: VRC01, VRC03, 3BNC117, N6, F105, PG9, PG16, PGT145, 10-1074, PGT121, 10E8, 7H6, 4E10, and 35O22; the psPAX2 plasmid; HIV-1 Subtype B Panel of SGA gp160 Env Clones (from B.H. Hahn, B.F. Keele and G.M. Shaw) and T20. We also thank D. Easterhoff, T. Bradley, and B. Haynes (Duke University) for providing the 902090 expression plasmids; J. Robinson (Tulane University) for the 17b, 19b, and JR52 expression plasmids; J. Mascola (NIH Vaccine research Center) for the VRC34 expression plasmids; R.W. Sanders and I. Del Moral Sanchez (University of Amsterdam) for providing the BG505 SOSIPv6 expressing plasmid; S. Pickthorn and T. Picard (University of Minnesota) for generating the CH040 T/F E279D mutant and helping to purify 1059 gp120; and G. Hart (University of Minnesota) for help with the flow cytometry. We thank L. Corey, J. Hural, N. Na (Fred Hutchinson Cancer Center), D. Montefiori (Duke University), those that sequenced the viral genomes, generated the expression plasmids and conducted the viral neutralization assays as well as the volunteers in the HVTN 704 trial for the Env-expressing plasmids from the antibody-mediated prevention trial (HVTN 704). We thank J. Vielmetter, P. Hoffman, and the Protein Expression Center in the Beckman Institute at Caltech for expression assistance. Some of the electron microscopy experiments were performed in the Caltech Cryo-EM Center with assistance from S. Chen and A. Malyutin. Cryo-EM data for the lectin-purified unliganded BG505-SOSIP and 1059-SOSIP were collected at the Duke Krios at the Duke University Shared Materials Instrumentation Facility (SMIF), a member of the North Carolina Research Triangle Nanotechnology Network (RTNN), which is supported by the National Science Foundation (award number ECCS-2025064) as part of the National Nanotechnology Coordinated Infrastructure (NNCI). A.H. is the recipient of an amfAR Mathilde Krim Fellowship in Basic Biomedical Research (108501-53-RKNT) and a phase II amfAR research grant (109285-58-RKVA) for independent investigators. This work was supported by an AIRP grant from the University of Minnesota Medical School (to A.H.; work on 1059 SOSIP), Avenir Award 1DP2DA049279-01 (NIH Director's New Innovator Award) from NIH/NIDA (to A.H.; work on HIV-1 evolution *in vivo*), National Institute of Allergy and Infectious Diseases (NIAID) U01 grant 1U01AI169587 (to A.H. (contact PI) and P.A. (work on 1059-SOSIP structure)), and NIAID R01 1R01AI167653 (to A.H.; work on N6 antiviral activity). The work was also supported by the NIAID Grant

HIVRAD P01 AI100148 (to P.J. Bjorkman), the Bill and Melinda Gates Foundation Collaboration for AIDS Vaccine Discovery (CAVD) grant INV-002143 (to P.J. Bjorkman), NIH P50 AI150464 (to P.J. Bjorkman), NIH R01 AI145687 (to P.A.) and NIH U54 AI170752 (to P.A.). The content is solely the responsibility of the authors and does not necessarily represent the official views of the NIH.

Author contributions

K.A.D., J.S. and A.H. designed the experiments; S.R., M.H., H.C., D.P., S.A. and A.H. performed the experiments. K.R.P., R.P., X.H., S.S., K.J. and P.A. performed the structural studies and analysis of unliganded 1059 and BG505 SOSIPs. K.A.D. performed the structural studies of 1059-SOSIP complexes and prepared the related figures; K.A.D and S.S. conducted SOSIP trimer nitroxide labeling. K.A.D, M.D.B. and W.L.H. designed and analyzed data for DEER experiments. M.D.B. collected and processed DEER data. S.R., H.C., K.A.D, J.S., P.A. and A.H. analyzed the data; A.H. wrote the paper with contributions from all authors.

Competing interests

A.H. is an inventor on a provisional patent application filed by the University of Minnesota for engineering 1059 SOSIP immunogens. Other authors declare no competing interests.

Methods

Cell lines

293T cells were purchased from the American Type Culture Collection (ATCC) and the TZM-bl cells were obtained from the NIH AIDS Reagent Program. Expi293F / 293F cells for protein expression were purchased from Gibco (ThermoFisher Scientific). Cf2Th-CD4/CCR5, Cf2Th-CCR5, and Cf2Th-CD4/CXCR4 were generated in the laboratory of Joseph Sodroski. Cell lines were not authenticated and were tested negative for contamination with mycoplasma.

Expi293F / 293F cells were maintained at 37 °C and 8% CO2 in Expi293 / 293F freestyle Expression medium (Gibco; ThermoFisher Scientific) with continuous shaking at 110-130 rpm. 293T and TZM-bl cells were grown in Dulbecco's Modified Eagle Medium (DMEM) containing 10% Fetal Bovine Serum (FBS), 100 µg/ml streptomycin and 100 units/ml penicillin. Cf2Th-CD4/CCR5 and Cf2Th-CD4/CXCR4 cells were grown in the same medium supplemented with 400 µg/ml G418 and 200 µg/ml hygromycin B (both from Invitrogen, ThermoFisher Scientific). Cf2Th-CCR5 cells were grown in the same medium supplemented with 400 µg/ml G418.

Plasmid construction

Expression plasmids for T/F Envs were obtained from the NIH AIDS Reagent Program. HIV-1_{JR-FL}, HIV-1_{CH040}, and HIV-1_{1059} *env* mutants were generated by site directed mutagenesis or by PCR assembly followed by Gibson Assembly into pcDNA3.1™(-)Zeo based vectors. Correct DNA sequences were verified by Sanger sequencing. CH040 *env* variants based on consensuses sequences of viruses that evolved over time in patient as well as the K160N and E332N CH040 *env* mutants were generated by site directed mutagenesis or gene synthesis (Gene Universal, Newark, DE). Codon-optimized 1059 SOSIP was synthesized and cloned into pTwist-CMV_Betaglobin_WPRE_Neo vector (by Twist Biosciences, San Francisco, CA); the vector was further modified to replace the natural signal peptide with the tissue plasminogen activator (TPA) signal peptide and to introduce stabilizing mutations (by Gene Universal, Newark, DE). Genes for expression of monomeric gp120s were codon-optimized and cloned into a pTwist-CMV_Betaglobin_WPRE_Neo vector that contained an 8-Histide tag at the C-terminus to facilitate purification by Ni-NTA chromatography (by Gene Universal, Newark, DE).

Production of recombinant HIV-1 expressing luciferase

We produced viruses by cotransfecting 293T cells with three plasmids: an envelope-expression plasmid, pHIVec2.luc reporter plasmid and psPAX2 packaging plasmid (catalog number 11348, NIH AIDS Reagent Program) in a ratio of 1:6:3 using either Effectene (Qiagen) or calcium phosphate, as previously described[63,64]. After a 48-hour incubation, the cell supernatant was collected and centrifuged for 5 minutes at 600-900x g at 4°C. The amount of p24 in the supernatant was measured using the HIV-1 p24 antigen capture assay (catalog number 5421, Advanced BioScience Laboratories or in-house p24 assay) and the virus-containing supernatant was frozen in single-use aliquots at -80°C.

Viral infection assay

A single-round infection assay was performed as previously described[7,63,65,66]. Briefly, HIV-1 Env ligands (antibodies and sCD4) were diluted in DMEM and thirty microliters of each tested concentration were manually dispensed into a well (with 2-3 replicates for each concentration) of a 96-well white plate (Greiner Bio-One, NC). Thirty microliters of viruses pseudotyped with specific Envs were then added, and after a brief incubation at room temperature, thirty microliters of $1.7x10^5$ Cf2Th-CD4/CCR5 target cells/ml in DMEM were added. We used either 2 ng of p24 of virus preparations or tittered the viruses on Cf2Th-CD4/CCR5 cells and used 1-3 million relative light units (2 sec integration using Centro LB 960 or Centro XS^3 LB 960 luminometer) on all experiments. After 48-72 hour incubation, the medium was aspirated and cells were lysed with 30 µl of Lysis Buffer. The activity of the firefly luciferase, which was used as a reporter protein in the viral assay, was measured with a Centro LB 960 (or Centro XS^3 LB 960) luminometer (Berthold Technologies, TN, USA).

To assess the effect of exposure to cold on virus infectivity, single-use aliquots of recombinant virus preparations were thawed at 37°C for 1.5 min at indicated intervals and then incubated on ice for different time periods. At the end of the incubation, equal amounts of recombinant viruses were added to Cf2Th-CD4/CCR5 target cells to assess infectivity.

Calculation of half maximal inhibitory concentration (IC_{50}) and infectivity decay on ice

Dose response curves of viral infection assay were fitted to the four-parameter logistic equation using Prism 7 program (GraphPad, San Diego, CA) after adding the equation to the program; IC_{50} values and the associated s.e. are reported[67–69]. Dose response curves of virus infectivity decay on ice were fitted to one phase exponential decay using the Prism 7 program. Number of experiment repeats and replicates are provided in Figure Legends.

Cell-cell fusion assay

Cell-cell fusion was monitored as previously described[70] but using HIV-1 tat as a transactivator and TZM-bl cells as reporter (target) cells. Briefly, 500,000 293T cells in each well of a 6-well plate were co-transfected with HIV Envs and HIV-1 tat expression plasmids at a ratio of 1:6 (total 2µg). After 48 hours, the cells were detached with 5mM EDTA/PBS, and 10,000 cells were added to each well of TZM-bl reporter target cells that were pre-seeded (10,000/well) the day before. Cells were incubated for the specified time and then lysed; luciferase activity was measured and used to evaluate the extent of fusion.

Flow cytometry

Binding of CD4bs bnAbs to HIV-1_{JR-FL} Envs expressed on the surface of 293T cells was analyzed by flow cytometry as previously described[7]. Briefly, 293T cells were transfected with an Env-expressing plasmid for expression of either HIV-1_{JRFL_WT} or HIV-1_{JRFL_L193R} Envs, which adopts a more open Env conformation[7]. Cytoplasmic tail of both expressed Envs was deleted (ΔCT) to allow a high level of Env expression to reliably measure CD4bs bnAb binding. Forty-eight hours after transfection, cells were detached with 5mM EDTA/PBS, washed, and 300,000 cells in 100 µl 5% FBS/PBS were incubated with 0.01 µg/ml of indicated bnAbs for 30 minutes. Cells were washed twice and incubated with Allophycocyanin (APC)-conjugated F(ab′)2 fragment

donkey anti-human IgG antibody (1:100 dilution; catalog number 709-136-149; Jackson ImmunoResearch Laboratories) for 30 minutes. Cells were washed twice and analyzed by CytoFLEX flow cytometer (Beckman Coulter) using CytExpert software. All procedures were performed at room temperature.

Protein expression and purification

sCD4. Plasmid containing a codon-optimized sCD4 gene was transfected into 293F cells using 293fectin transfection reagent (Invitrogen, Thermo Fisher Scientific Inc.). Transfected cells were grown for 3-6 days at 37°C and 8% CO_2 with continuous shaking and the secreted proteins, all of which contained a 6-histidine tag at their C-terminus, were purified from the culture supernatant using Ni-NTA chromatography[71]. Binding of sCD4 to the Ni-NTA column was weak and therefore to allow efficient binding we did not add a low concentration of imidazole to the supernatant prior to sCD4 purification.

Monomeric gp120. 293F cells were transfected with a gp120-expressing plasmid using Turbo293 transfection reagent (Speed Biosystems; Gaithersburg, MD) and grown for 3-5 days in a tissue culture incubator at 37°C, 8% CO_2 with continuous shaking. Culture supernatant containing soluble gp120 glycoprotein was then clarified by centrifugation at 7000 x g for 1 hour and filtered using a 0.45 µm vacuum filtering system (VWR). Supernatant was dialyzed against Ni-NTA buffer (50 mM NaH_2PO_4, 300 mM NaCl; pH 8.0) overnight using a 13,000 MWCO dialysis tube (VWR) and the dialyzed supernatant was loaded on a column of Ni-NTA agarose beads (Qiagen) at 4-8°C. The column was washed with 500 mM NaCl in phosphate buffered saline pH 8.0 and the gp120 glycoprotein was stepwise eluted with Ni-NTA buffer containing 50-250mM imidazole (MilliporeSigma) solutions. Elution fractions were analyzed on 8–16% SDS-PAGE (mini-PROTEAN TGX protein gels; Bio-Rad) and fractions containing the gp120 glycoprotein were concentrated followed by buffer exchange to PBS using Vivaspin 6 centrifugal concentrators (30kDa; Cytiva). Purified gp120 glycoproteins were flash frozen and stored in aliquots at -80°C.

SOSIP trimers. 293F cells were co-transfected with a SOSIP-expressing plasmid and a human furin-expressing plasmid at a 4:1 ratio (4 SOSIP : 1 furin) using polyethyleneimine (PEI; Polysciences, Inc. Warrington, PA). Transfected cells were grown for 3-5 days in a tissue culture incubator at 37°C, 8% CO_2 with continuous shaking and culture supernatant was then clarified by centrifugation at 4000 x g for 20 minutes and filtered using 0.2 µm vacuum filtering system (VWR). SOSIP glycoproteins were purified from the supernatant by affinity chromatography and further by size exclusion chromatography as follows. Filtered culture supernatant was loaded on *Galanthus nivalis* lectin column (Vector Laboratories) at 4°C or in ice and washed with 2-3 column volumes of 500 mM NaCl in phosphate buffered saline pH 8. SOSIP glycoproteins were eluted with 1M methyl-α-D-mannopyranoside (from Vector Laboratories or MilliporeSigma), filtered through 0.2 µm filter and concentrated using Vivaspin 6 centrifugal concentrators (30kDa; Cytiva). Purified SOSIP glycoproteins were then separated on a HiLoad 16/600 Superdex 200 pg size exclusion chromatography column (Cytiva) and fractions corresponding to SOSIP trimers were pooled, concentrated, and stored in aliquots at -80°C.

Genes encoding the 1059 SOSIP proteins used in some single-particle cryo-EM datasets (Class I 1059-17b, Class II 1059, 1059-N6-10-1074) and DEER experiments were co-expressed with a plasmid encoding furin using the Expi293 transient transfection system (ThermoFischer). Trimeric Envs were separated from cell supernatants using 2G12 immunoaffinity chromatography and subsequently purified by size exclusion chromatography using a Superose 6 10/300 column (Cytiva), as previously described [72–74].

We purified SOSIP by 2G12 immunoaffinity chromatography for structural studies in which 1059-SOSIP was incubated with different Fabs and used 1059 and BG505 SOSIP purified by *Galanthus nivalis* lectin chromatography, which exploits lectin binding to Env surface glycans in a conformation-independent manner, for determining unliganded SOSIP structures. The latter method is expected to include SOSIP trimers that bind and those that do not bind 2G12. All preparations were further purified by size-exclusion chromatography and cryo-EM data processing methods were used to robustly exclude misfolded SOSIP trimers as described in the sections below.

Enzyme-linked immunosorbent assay (ELISA)

We used ELISA to analyze antibody binding to SOSIP trimers. Env-specific capturing antibody JR52 was immobilized in wells of a high binding, flat-bottom 96-well plate (Greiner Bio-One, NC) by adding 0.4μg of JR52 in 100 μl PBS in each well and incubating the plates overnight at room temperature (RT). Next, the wells were washed 3 times with PBS containing 0.2% Tween-20 (wash solution) using in-house vacuum system and blocked with PBS containing 3% bovine serum albumin (blocking solution) for 2 hours at RT. The wells were then washed 3 times, 0.25-0.5 μg of purified SOSIP trimers in blocking solution were added to test wells and the plate was incubated for 2 hours at RT. Wells were washed 6 times and specified antibodies were added at different concentrations. After 1 hour and 30 minutes incubation, wells were washed 6 times and 1:5000 dilution of horseradish peroxidase (HRP)-conjugated donkey anti-human IgG (FC specific; Jackson ImmunoResearch Laboratories, West Grove, PA) was added in blocking solution to each well and the plate was incubated for 1 hour at RT. Wells were then washed 6 times and 100 μl of TMB solution (1 ml of 1 mg/ml 3,3,5,5-tetramethylbenzidine (MIlliporeSigma) in DMSO, 9 ml of 0.1 M sodium acetate, pH 5.0, and 2 μl of fresh 30% hydrogen peroxide) were added to each well. After ~18-minute incubation, the HRP reaction was stopped by adding 50 μl of 0.5 M H_2SO_4 and optical density at 450 nm was measured using Synergy|H1 microplate reader (BioTek). Binding to 1059 SOSIP open conformation was measured in a similar manner, but we immobilized 17b (or 2G12 or 10-1074 controls) antibody to capture 1059 SOSIP, and used biotinylated N6, which was prepared according to manufacturer's instructions (EZ-Link™ Sulfo-NHS-LC-Biotinylation Kit; ThermoFisher Scientific), followed by streptavidin-HRP to detect N6 bnAb binding. In separate experiments, we used 17b Fab to capture 1059 SOSIP open conformation and detected bnAb binding with HRP-conjugated donkey anti-human IgG as described above. For experiments involving glutaraldehyde cross-linking, wells were incubated with 5mM glutaraldehyde in DDW for 15 min followed by blocking with 25mM glycine solution. In some experiments, monomeric gp120s and SOSIPs were immobilized through soluble *Galanthus nivalis* lectin (Vector Laboratories) and all subsequent steps were performed as described above.

Western blot

gp120 or SOSIP glycoproteins were separated on 8–16% SDS-PAGE (mini-PROTEAN TGX protein gels; Bio-Rad) and transferred to a 0.45 µm nitrocellulose membrane (catalog number 1620115, Bio-Rad). The membrane was blocked with 5% blotting-grade blocker (catalog number 1706404, Bio-Rad) in PBS (5%MPBS), washed with PBS, and incubated for 1-hour on a shaker with serum from a person living with HIV-1 (1:30,000 dilution) and sheep anti-gp120 IgG (1:30,000 dilution; catalog number 288, NIH AIDS reagent program) both diluted in 5%MPBS. After 3 washes with 0.05% Tween 20 (catalog number 1706531, Bio-Rad) in PBS (TPBS), the membrane was incubated with peroxidase conjugated anti-human IgG (1:10,000 dilution) and anti-sheep IgG (1:10,000 dilution) (Jackson Immunoresearch) in 5%MPBS for 1-hour. The membrane was washed 3 times with TPBS, developed with SuperSignal West Pico PLUS Chemiluminescent Substrate (catalog number 34580, ThermoFisher Scientific), and analyzed using the Odyssey imaging system (LI-COR Biosciences). In some cases, we used serum from a person living with HIV-1 (1:10,000 dilution) without sheep anti-gp120 IgG.

Biolayer interferometry

Binding kinetics was measured on an Octet RED96e system (ForteBio) at 25°C with shaking at 1,000 RPM using Protein A (ProA) biosensors (ForteBio). The biosensor tips were hydrated for 60 sec with kinetic buffer and loaded with monoclonal antibodies (mAbs) 17b or N6 (diluted in kinetic buffer at 12.5 µg/mL) for 60 sec. Loaded tips were then placed in a kinetic buffer for 120 sec for baseline equilibration. Association phase of soluble Env trimer (BG505 SOSIP or 1059 SOSIP) binding to mAbs was measured for 180 sec at various concentrations ranging from 100 nM to 3.125 nM (a two-fold dilution series) SOSIPs in kinetic buffer. Dissociation was measured for 300 sec. Baseline was subtracted from all data prior to curve fitting to a 1:1 binding model using ForteBio data analysis software. Interactions were fitted with a single global Rmax parameter (maximum response), imposing a stringent restriction on the fit.

Pulsed DEER spectroscopy

V1 spin labeling of 1059 SOSIP. In this study, spin labeling sites were selected based on characterization in previous work[30]. Each site represents a solvent-exposed residue that is within a defined secondary structure (β strand or α-helix) and not in flexible loops. The size of the V1 label is similar to the size of an amino acid and, thus, the label size and rotations (rotamers) minimally contribute to DEER distance distributions (several angstroms)[30]. The radical center V1 is found within the nitroxide ring, not the peptide linkage. Collectively, these factors should be taken into account and suggest DEER results can be complicated by conformationally heterogeneous and intrinsically flexible proteins of interest. V1 spin labeling and pulsed DEER spectroscopy of SOSIPs were preformed similarly to procedures previously described[30]. Purified SOSIPs were concentrated to ~100 µM in TBS, pH 7.4, and tris(2-carboxyethyl)phosphine (TCEP) reducing buffer was added in a 2-fold molar excess relative to the target cysteine. SOSIPs were reduced for one hour at room temperature, then TCEP was removed using a Zeba desalting column (TheroFisher Scientific). The V1 nitroxide spin label (bis(2,2,5,5-tetramethyl-3-imidazoline-1-oxyl-4-il)-disulfide) was added at a five-fold molar excess relative to target cysteines and incubated at room temperature for five hours, then 4°C overnight. Excess V1 spin label was removed using

size exclusion chromatography (Superose 6 10/300 column; Cytiva). V1-labeled SOSIP was buffer exchanged into deuterated buffer containing 20% glycerol. For CD4-liganded SOSIPs, V1-labeled SOSIPs were incubated at a 3-fold molar excess[75] of CD4 for five hours at room temperature. All samples were stored at 4°C before flash freezing. As a control we used WT HIV-1 1059 SOSIP Envs that did not contain mutations to cysteines. This control was subject to the labeling process but did not produce DEER signal.

DEER spectroscopy setup and measurements. Fifty-eight µL samples of 25-50 µM spin-labeled protein complexes were flash frozen within a 2.0/2.4 mm borosilicate capillary (Vitrocom, Mountain Lakes, NJ) in liquid nitrogen. A closed-loop helium cryocooler and compressor system (Cold Edge Technologies, Allentown, PA) was employed to maintain a sample temperature of 50 K (-223.15 °C). Four-pulse Q-band DEER spectroscopy data were collected on a Bruker ELEXSYS 580 spectrometer equipped with an E5106400 cavity resonator (Bruker Biospin). Pulses were generated by a Bruker arbitrary waveform generator and amplified by a 150-watt TWT amplifier (Applied Engineering Systems, Fort Worth, TX) and pulse lengths were optimized via nutation experiment based on bandwidth (ranging from 15 to 21 ns (π/2) and 30 to 42 ns (π)). Observer frequency was set to a spectral position 2 G downfield of the low and central resonance intersection minimum in the absorption spectrum, and the pump envelope frequency was a chirp pulse resulting in a 50 MHz half-width square excitation 70 MHz downfield/up-frequency from the observer. Maximum dipolar evolution (DE) times ranged from 3 to 3.5 µs. Both the primary echo and continuous wave EPR signal amplitudes were low compared to what was expected from the protein concentration. This indicates that the protein is under-labeled, which is not unexpected for the V1 spin label because of dissociation from the protein[76]. Thus, the concentration of spin pairs was low, resulting in low signal-to-noise (*ca.* 3-10 after background correction) and contributing to a low modulation depth (*ca.* 0.05-0.15) in the DE data. Low modulation depths can also have contributions from a fraction of pairwise spin interactions outside of the detectable limit of DEER[41], which may be the case here based on the structures and locations of some of the spin labels (e.g., 1059-202* interprotomer distances in the +sCD4 case, PDB:5VN3). Nevertheless, the DE data clearly reveal pairwise interactions within the detectable limits of the DEER technique, and the data were analyzed to determine inter-spin distance distributions with the program LongDistances v.1020, written by Christian Altenbach (Christian Altenbach. LongDistances - A Program to Analyze DEER Data. EPR Newsletter of the international EPR (ESR) Society, 31/2:12-13, 2021).

DEER spectroscopy analysis. The LongDistances DEER analysis software is available online (http://www.biochemistry.ucla.edu/biochem/Faculty/Hubbell/). The Model-Free distance distributions were fit with the 3D background co-refinement option enabled, and with all other default fitting parameters employed. The resulting distance distributions were evaluated for reliability by determining the range of populations permitted by the data at a given distance, considering the signal-to-noise, depth of modulation and other features. This “error analysis” (plots provided in Extended Data Fig. 10) is essentially the probability that a population at a given distance determined by the fit is meaningful. Distance distribution data comparing unliganded and sCD4-bound mutants (Fig. 2f) were normalized according to relative total areas and depths of modulation, for direct comparison of their spin pair populations[30]; distances beyond the vertical grey dotted line on each plot are unreliable based on dipolar evolution duration[41].

Assembly of protein complexes and Cryo-EM sample preparation for Class I 1059-17b, Class II 1059, and 1059-N6-10-1074 datasets

Protein complexes used for cryo-EM were created by incubating Fabs (17b, N6, and/or 10-1074) with SOSIP Envs (that were purified using 2G12 immunoaffinity chromatography) in a 3:1 ratio for five hours at room temperature, then 4°C overnight. Each complex was purified using size exclusion chromatography (Superdex 200 1/150 column; Cytiva) and the peak corresponding to the complex was pooled and concentrated to 3.5 mg/ml. Cryo-EM quantifoil R2/2 300 mesh grids (Ted Pella) were glow discharged at 20 mA for 1 minute using a PELCO easiGlow (Ted Pella). Immediately prior to applying 3.0 µL of the complex to the grids, fluorinated octyl maltoside (FOM) was added to samples at a final concentration of 0.02% (w/v). Cryo-EM grids were blotted using Whatman No. 1 filter paper for 3-4 sec and plunge frozen in liquid ethane using a Mark IV Vitrobot (ThermoFisher Scientific) operating at 22°C and 100% humidity.

Cryo-EM Data collection and processing for Class I 1059-17b, Class II 1059, and 1059-N6-10-1074 datasets

Single particle cryo-EM data was collected using a 200kV Talos Artica electron microscope (ThermoFisher Scientific) equipped with a K3 camera (Gatan) operating with super-resolution mode at 0.869 Å•pixel-1 (1059-N6-10-1074 complex) or a 300kV Titan Krios electron microscope (ThermoFisher Scientific) equipped with a K3 camera (Gatan) and GIF Quantum energy filter (20eV slit width) operating at 105kx magnification with super-resolution mode at 0.855 Å•pixel-1 (1059-17b complex). For both datasets, the defocus range was set at 1.0-3.0 µm. SerialEM v3.7 software was used to collect movies that were sectioned into 40 subframes with a total dose of $60e^{-}$•$Å^{-2}$ generating a dose rate of $1.5e^{-}/Å^{2}$•subframe. A total of 2,744 and 10,738 movies were collected for 1059-N6-10-1074 and 1059-17b complex, respectively.

Data processing for 1059-N6-10-1074 complex was performed using cryoSPARCv2.15.0 (ref[75]). Movies were binned and patch motion was corrected for beam-induced motion, including dose weighting. CTF estimation using non-dose-weighted images was performed using CTFFIND v4.1.14 (ref[77]) and movies were curated to exclude images with poor CTF fits or crystalline ice. The Blob picker was used to select reference-free particles, which were subsequently un-binned, extracted, and subjected to multiple rounds of 2D classification. Class averages representing the desired complex were selected and used to generate an ab-initio model. The ab-initio model was used as an initial model for non-uniform refinement that generated the final map, which was determined to be C3 symmetrical by the phenix map_symmetry function[78] and processed as such. Data processing for 1059-17b complex was performed using RELION[79]. MotionCor2 (ref[80]) was used to motion-correct movies after binning, then CTFFIND v4.1.14 (ref[77]) was used to estimate CTF. Again, movies were curated to exclude images with poor CTF fits or crystalline ice. Subset of particles were manually picked and used for reference-free 2D classification. Classes representing the desired complex were used as references for RELION AutoPicking[79,81]. 2D classes were generated and particles in classes representing the desired complex were selected for 3D classification. Prior, low-resolution maps (unpublished data) were used as a reference for 3D classification. 3D classification revealed two distinct classes, Class I with the desired 1059-17b complex and

Class II with 1059 unliganded. 3D classes representing each class were combined and underwent 3D auto-refinement and post-processing. Particles from each class used for 3D auto-refinement were un-binned and re-extracted, then subjected to 3D classification using 3D auto-refinement maps from binned particles as a reference. Map symmetry was identified using phenix map_symmetry function[78] which determined Class I and Class II maps contained C3 symmetry. Therefore, downstream processing applied C3 symmetry. 3D classes representing the desired class were selected and subjected to 3D auto-refinement and post-processing. For the 1059-17b complex, Fab C_HC_L domains were masked out. Each class then underwent iterative rounds of particle CTF refinement, particle polishing, 3D auto-refinement, and post processing until the final maps were generated.

Remote 3DFSC Processing Server[81] was used to generate 3D FSCs of maps which calculated resolutions using gold-standard FSC 0.143 criterion[81]. Local resolutions of the refined maps were generated using cryoSPARC[75] or RELION[79].

Cryo-EM Data collection and processing for unliganded 1059 and BG505 SOSIPs (purified by GLN/SEC)
Sample concentrations used were 2.16 mg/mL for 1059-SOSIP and 3.64 mg/mL for BG505-SOSIP. To prevent interaction of the trimer complexes with the air-water interface during vitrification, the samples were incubated in 0.085 mM n-dodecyl β-D-maltoside (DDM) before vitrification. Samples were applied to plasma-cleaned QUANTIFOIL holey carbon grids (EMS, R1.2/1.3 Cu 300 mesh) followed by a 30 second adsorption period and blotting with filter paper. The grid was then plunge frozen in liquid ethane using an EM GP2 plunge freezer (Leica, 90-95% relative humidity). Cryo-EM data were collected using a 300 kV FEI Titan Krios electron microscope (ThermoFisher Scientific) equipped with a K3 camera (Gatan) and GIF Quantum energy filter (20eV slit width) operating at 81kx magnification with a pixel size of 1.08 Å. Gatan latitude software was used to collect a total of 13,405 and 14,296 movies for the 1059-SOSIP and the BG505-SOSIP structures, respectively.

The data were processed in cryoSPARCv4.01(ref[75]). Movies were aligned using Patch Motion Correction and the non-dose weighted aligned micrographs were used for the CTF correction with PatchCTF Estimation. In the first round of particle selection, particles were picked with a box size of 280 Å using the Blob picker with a circular blob having a maximum diameter of 240 Å and these particles were subjected to multiple rounds of 2D classification. The 2D class-averages that best represent the views of 1059-SOSIP glycoprotein structure were selected as templates for the second round of particle selection using the Template picker. Subsequently, these particles were also subjected to multiple rounds of 2D classification yielding few more hundred particles than the Blob picker. The best 2D class averages were selected and processed by generating multiple classes of ab-initio models and followed by heterogeneous classification. 3D classes corresponding to 1059-SOSIP structure were selected and merged as they represent similar structures with small local changes and performed non-uniform refinement and followed by local refinement with C1 symmetry to yield one final map with global resolution of 3.6 Å (Extended Data Fig.6) at the gold-standard FSC 0.143 criterion. Remote 3DFSC Processing Server[81] was used to generate 3D FSCs of maps which calculated resolutions using gold-standard FSC 0.143 criterion[81]. Local resolutions of the refined maps were generated using cryoSPARC[75] . Similar procedures were used for the data

collection and processing of unliganded BG505 SOSIP. After the data processing, unliganded BG505 SOSIP data set resulted in 975,399 particles refined with C1 symmetry and yielded a final map with global resolution of 3.7 Å (Extended Data Fig. 6) at the gold-standard FSC 0.143 criterion. For conformational flexibility and asymmetry level analysis, both the unliganded 1059 and BG505 SOSIP datasets were subclassified by 3D variability and reconstructed 10 subclasses ranging from resolution of 3.7-4.3 Å (Extended Data Table 4).

Model fitting

The initial homology model of the 1059-SOSIP Env was constructed using the Modeller software[82] utilizing the template PDB 7LX2. Similarly, for the BG505-SOSIP Env, PDB ID 4ZMJ was used as an initial model. These models were fitted into their respective maps using UCSF ChimeraX[83]. Coot[83] and Isolde[84] were used to fix clashes and Ramachandran outliers, as well as to add glycans. Refinement was done using real-space refinement in Phenix[78] using global minimization, NQH flips, local grid search, secondary structure restraints, Ramachandran restraints and a nonbonded weight of 1000.

For conformational flexibility and asymmetry analysis, the respective final models were rigid fitted using real space refinement in Phenix[78] into ten subclasses of unliganded 1059 and BG505 SOSIPs. These models were used to calculate the interprotomer distance analysis and root mean square deviation to compare the asymmetry and flexibility respectively in unliganded 1059 and BG505 SOSIPs. Asymmetry level of each subclass was calculated using the following equation:

Asymmetry_{343} level = $|\text{Prot}_{AB} - \text{GeoM}| + |\text{Prot}_{BC} - \text{GeoM}| + |\text{Prot}_{CA} - \text{GeoM}|$

Prot_{xy} = the distance between residue 343 of protomer X and residue 343 of protomer Y in each subclass.

GeoM = geometric mean of 3 distances between residue 343 of all 3 protomers (AB, BC, and CA) in the final structure reconstructed from all particles for each related strain ($\text{GeoM}_{1059\text{-SOSIP}}$ = 92.47 Å; $\text{GeoM}_{BG505\text{-SOSIP}}$ = 93.17 Å). All calculations are provided in Supplementary Table 3.

Motion analysis

The density motion analysis of unliganded 1059 and BG505 SOSIPs was performed using 3D Variability analysis as previously described[85]. The analysis used the consensus pose of the complete unliganded 1059 SOSIP cryo-EM dataset containing 737,588 particles. Similarly, in case of BG505 SOSIP, the analysis used the consensus pose of the complete unliganded BG505 SOSIP cryo-EM dataset containing 975,399 particles. Three principal component variability modes were calculated for each dataset using the default options and the low-pass filter resolution was set to 5 Å. The movies are shown in the supplementary movies 1 and 2.

Structural analyses

Structure figures and movies were created using PyMOL (Schrödinger) and UCSF ChimeraX[86]. Structure models were fit in maps by rigid body fit.

Data availability

Data are available upon request. The cryo-EM maps a have been deposited in the Electron Microscopy Data

Bank (EMDB) under the following accession codes: EMD-41246 for unliganded 1059 SOSIP, EMD-41244 for unliganded BG505 SOSIP, EMD-26264 [https://www.ebi.ac.uk/pdbe/entry/emdb/EMD-26264] for 1059-17b (class I), EMD-26265 [https://www.ebi.ac.uk/pdbe/entry/emdb/EMD-26265] for 1059 (class II), EMD-26266 [https://www.ebi.ac.uk/pdbe/entry/emdb/EMD-26266] for the 1059-N6-101074 complex. The refined coordinates have been deposited in the RCSB database under the following accession codes: PDB ID 8TGW for unliganded 1059-SOSIP and PDB ID 8TGU for unliganded BG505-SOSIP.

Conformational flexibility of HIV-1 envelope glycoproteins modulates transmitted / founder sensitivity to broadly neutralizing antibodies

Extended Data Figures and Tables

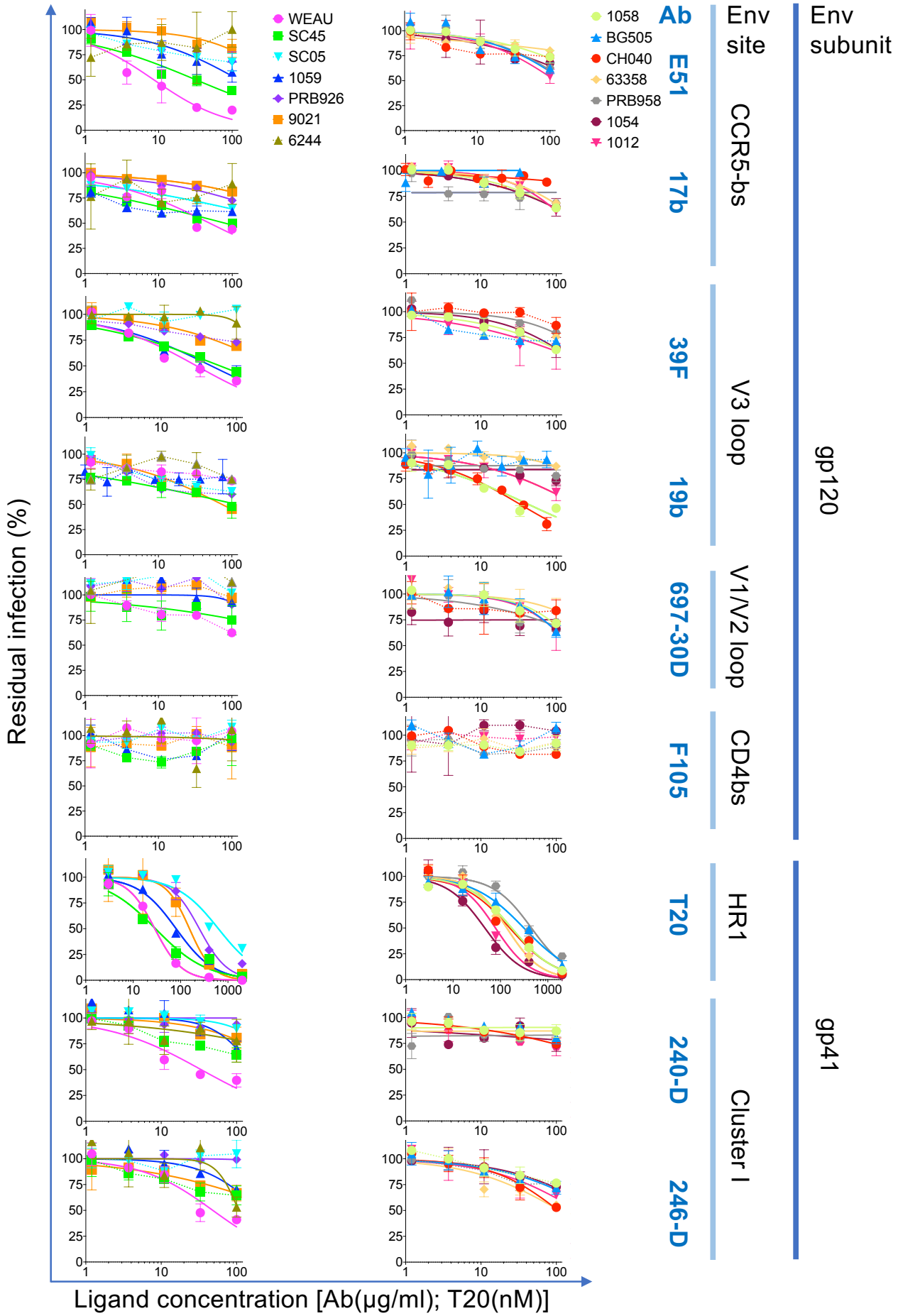

Extended Data Fig. 1. Sensitivity of HIV-1 pseudotyped with transmitted/founder (T/F) Envs to ligands preferentially recognizing internal epitopes. BG505, a control. Dashed lines connect data that could not be fitted to a standard inhibition curve. Data are average results of 2 independent experiments performed in duplicate ± SD except for 6244 data, which represent one of 2 independent experiments.

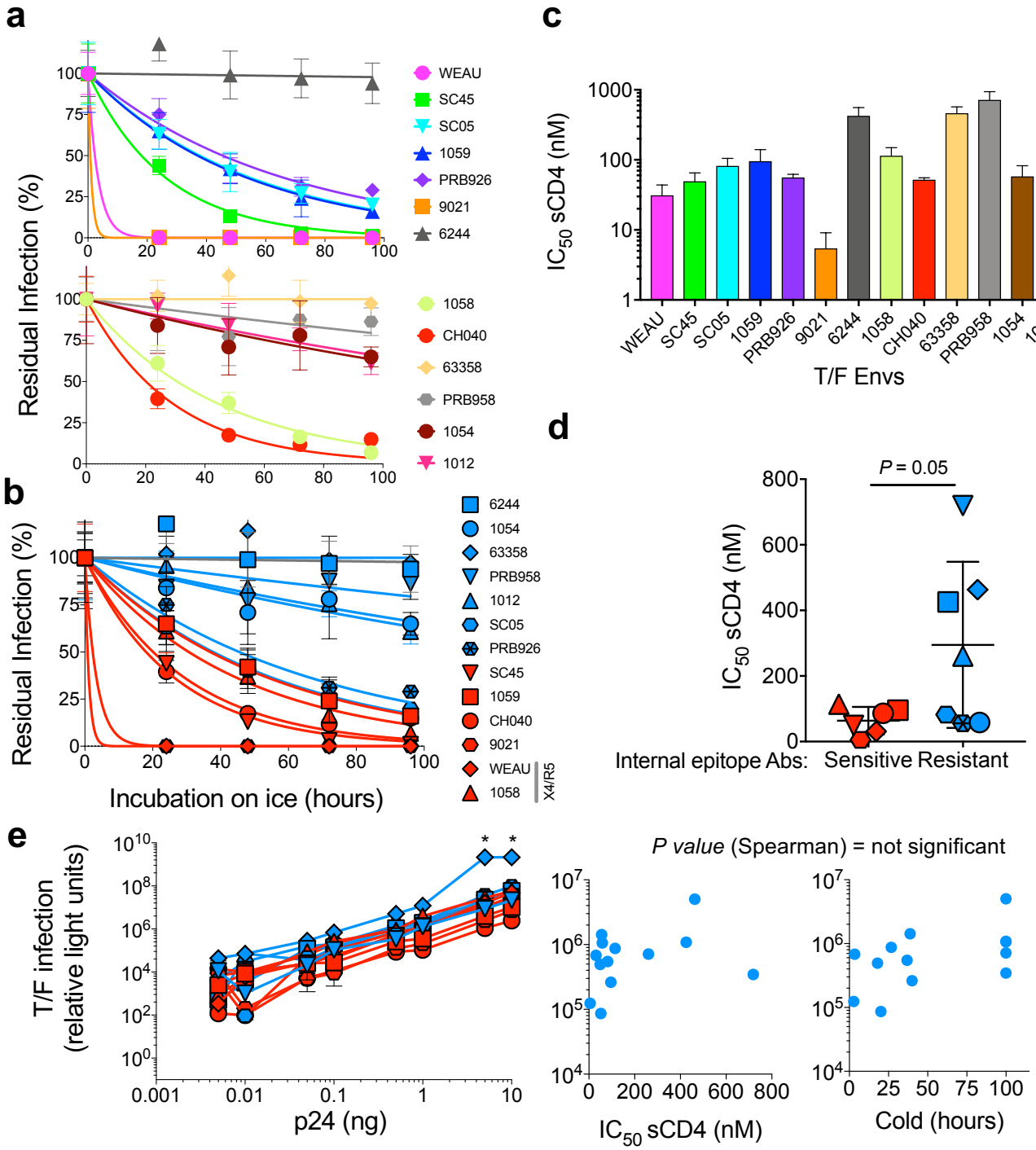

Extended Data Fig. 2. HIV-1 T/F Env sensitivity to cold exposure and soluble CD4 (sCD4). a, We assessed sensitivity of 13 T/F Envs to cold exposure by measuring viral (pseudoviruses) infectivity after pre-incubation of the pseudoviruses on ice for the indicated times. **b,** Similar to (**a**) but T/F Envs were plotted on a single plot and color coded according to sensitivity to internal-epitope antibodies. Blue, resistant Envs (up to 100 μg/ml); red, Envs that were inhibited by 50% or more by at least one antibody at up to 100 μg/ml concentration. Two dual-tropic (X4/R5) T/F Envs in this group are indicated in panel (**b**) legend. **c,** Sensitivity of HIV-1 pseudotyped with 13 T/F Envs to sCD4. Half maximal inhibitory concentrations (IC_{50}s) were calculated from dose response curves of pseudoviruses to increasing concentration of sCD4. **d,** Statistical analysis of difference between sCD4 sensitivity of T/F Envs that are sensitive and those that are resistant to internal-epitope antibodies. **e, Controls.** Left - we measured comparable infection levels of Cf2Th-CD4/CCR5 target cells by HIV-1 pseudotyped with 13 T/F Envs regardless of their internal-epitope exposure. Right - we did not detect statistically significant correlation between T/F viral infectivity and sCD4 or cold sensitivity. Color codes in panels **d** and **e (left)** are identical to the code in panel **b**. Asterisk, upper limit of light unit detection. *P,* calculated two-tailed Student's t-test *P* value. Data shown are representative (a-b,e) or average (c-d) results of at least two independent experiments, each performed in duplicate or triplicate.

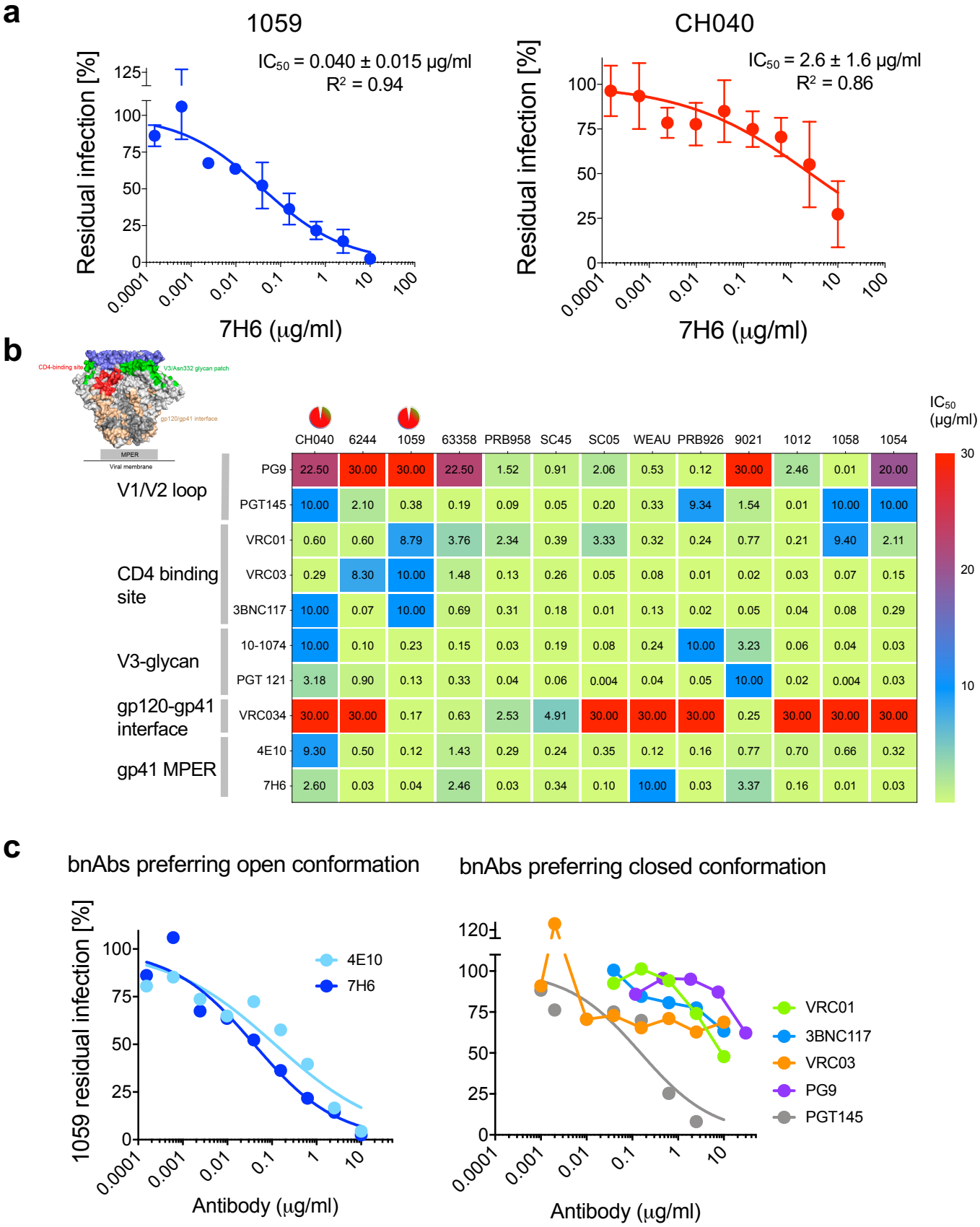

Extended Data Fig. 3. HIV-1 T/F Env sensitivity to bnAbs. a, Dose response curves of the sensitivity of viral entry, mediated by two T/F Envs, to the gp41-directed 7H6 bnAb. **b,** We calculated from dose response curves the IC_{50} values for the sensitivity of 13 T/F Envs to bnAbs of all known classes. 10.0 or 30.0 values represent values >10 or >30 μg/ml, respectively. Figure showing bnAb target sites on HIV-1 Env structure was adapted from Zhang *et al.*, Int. J. Mol. Sci. 2016. **c**, Dose response curves of the sensitivity of viral entry mediated by 1059 Envs to bnAbs that prefer specific Env conformations. Data shown are the average results of at least two independent experiments, each performed in duplicate.

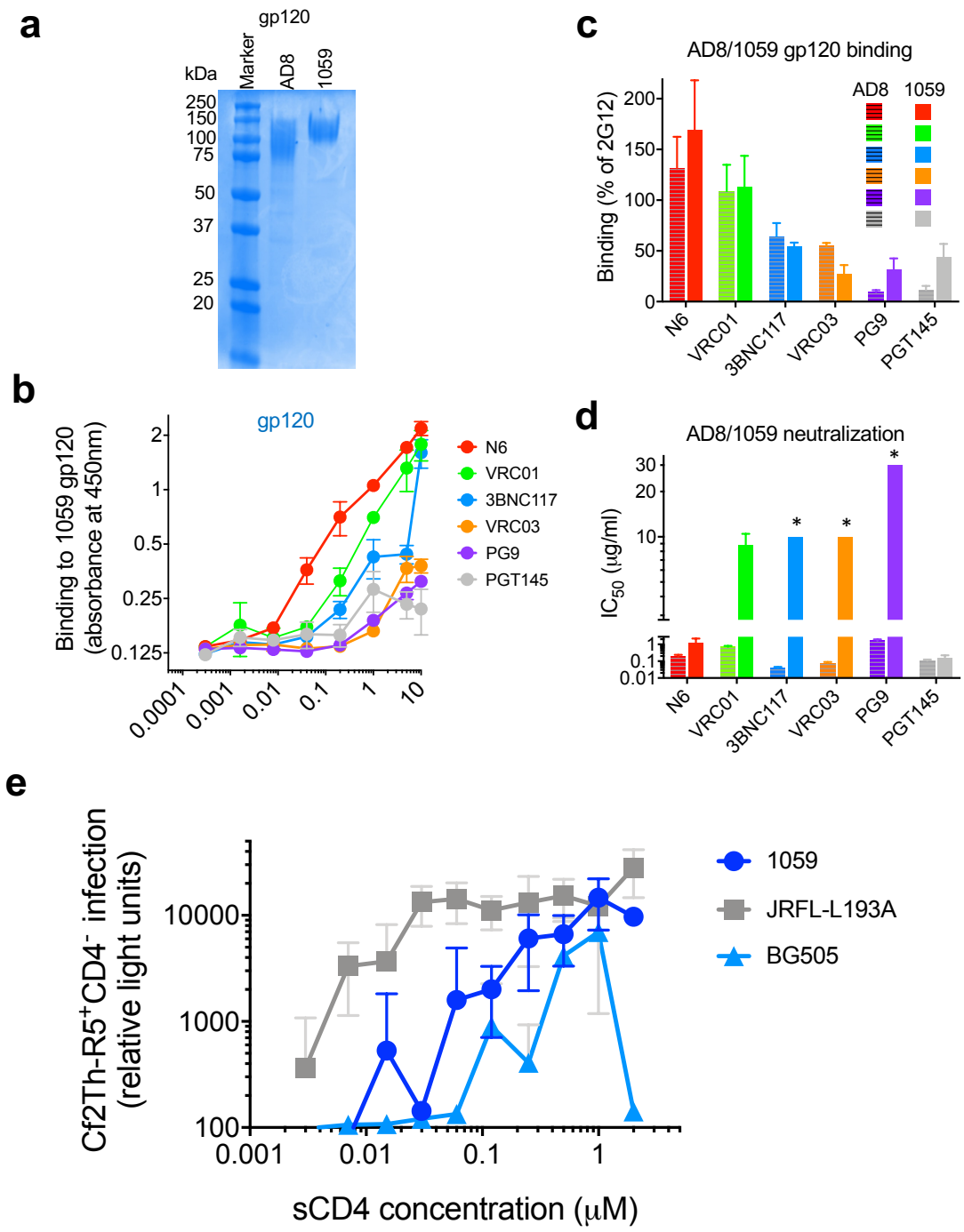

Extended Data Fig. 4. Antibody binding to soluble gp120 and CD4 dependence of HIV-1 Env-mediated entry. a, SDS-PAGE of purified 1059 gp120 **b**, Binding of CD4bs and V1V2 bnAbs to soluble 1059 gp120. **c**, Comparison of CD4bs and V1V2 bnAbs binding (1 μg/ml) to soluble gp120 of AD8 and 1059. **d,** Comparison of AD8 and 1059 pseudovirus neutralization by bnAbs from (**c**). Color code and bnAb order in panels **c** and **d** is identical. *, IC_{50} > maximal value tested. Data are average + SEM of at least 2 independent experiments, each performed at least in duplicate. **e**, We incubated recombinant pseudoviruses carrying the different Envs with CD4-negative, CCR5-expressing Cf2Th cells in the presence of indicated concentrations of sCD4. Between 48-72 hours post infection we measured the activity of firefly luciferase reporter protein (relative light units) to assess viral entry. Data shown are representative results from one of 2 independent experiments performed in triplicate ± standard deviation (SD).

a

	Signal peptide	Changes	501C-605C	I559P	R6	dMPER	64K	73C-561C	201C-433C	316W	535M	658V
SOSIP.664												
v4.1	Natural	64K, 316W										
DS	Natural	201C-433C										
v5.2.8a	Natural	64K,73C-561C,201C-433C, 316W,658V										
TPA WT	TPA											
TPA P22A	TPA-P22											

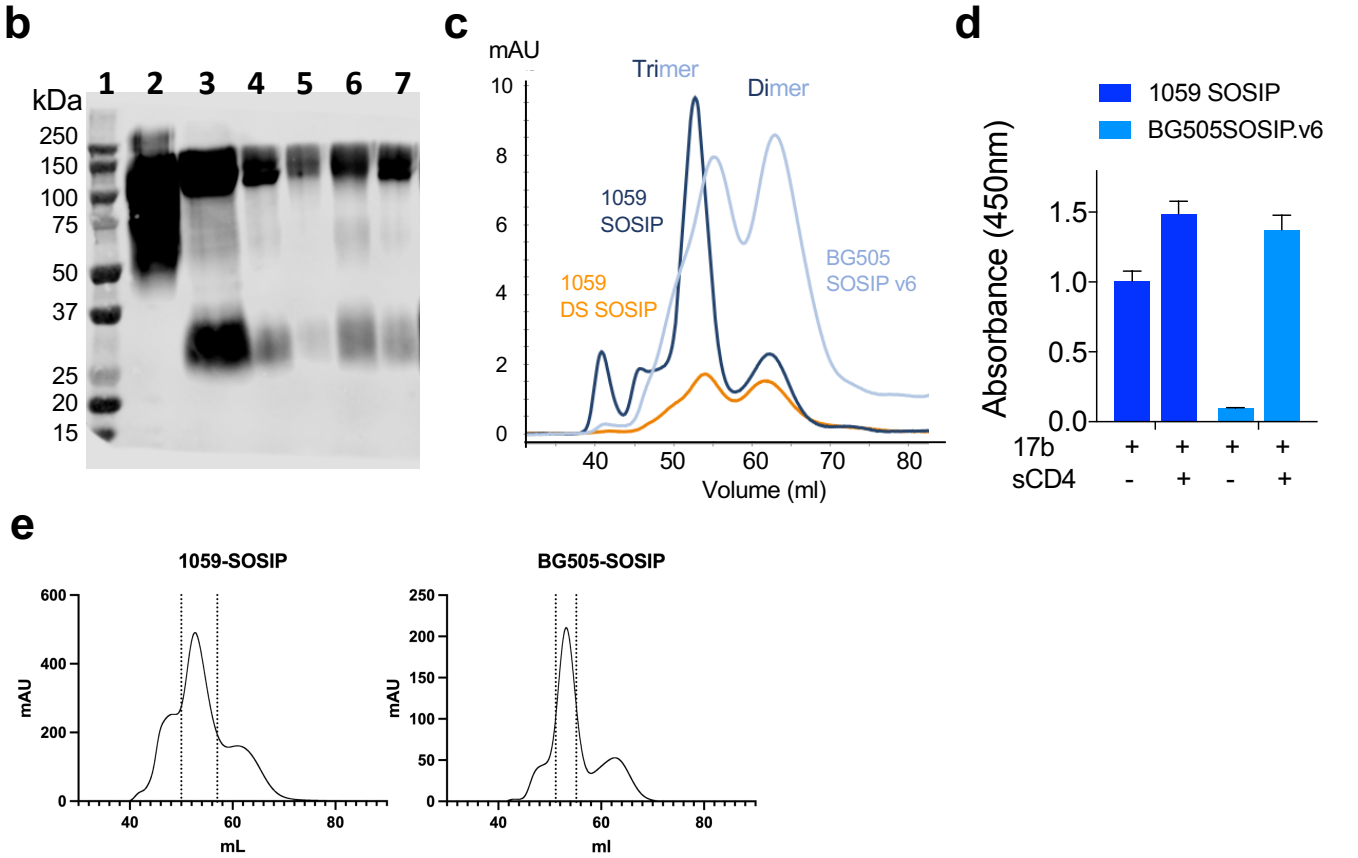

Extended Data Fig. 5. soluble 1059 SOSIP Env variants. a, We designed different 1059 SOSIP variants based on published studies and current knowledge. Env changes associated with each variant are shown and highlighted in green relative to the WT (red). **b,** Western blot of different 1059 SOSIP variants expressed in 293F cells for 4 days and analyzed directly from cell supernatants. We detected the SOSIP Env proteins using 1:10,000 dilution of serum of PLWH + 0.5μg/ml of JR52 antibody, which recognizes the D7324 epitope, followed by anti-human (1:10,000 dilution) + anti-mouse (1:20,000 dilution), both conjugated to horseradish peroxidase (HRP). Lanes: 1, ladder; 2, HIV-1_{AD8} gp120 control; 3, TPA WT; 4, TPA P22A (contains amino acid Alanine at position 22); 5, DS; 6, V5.2.8a; 7, v4.1. TPA, signal peptide of the Tissue Plasminogen Activator. TPA-1059 SOSIP exhibited the highest expression levels and was selected for further characterization in all studies described in the main text. **c,** Comparison of size exclusion chromatography (SEC) profile of 1059 and BG505 SOSIP v6 trimers (both contained the signal peptide derived from the TPA). **d,** ELISA of 17b antibody binding to 1059 and BG505 SOSIPs in the presence and absence of sCD4. **e**, SEC profiles of 1059-SOSIP and BG505-SOSIP preparations used for determining structures of the unliganded Envs. The dashed vertical lines indicate the fractions that were pooled for downstream studies.

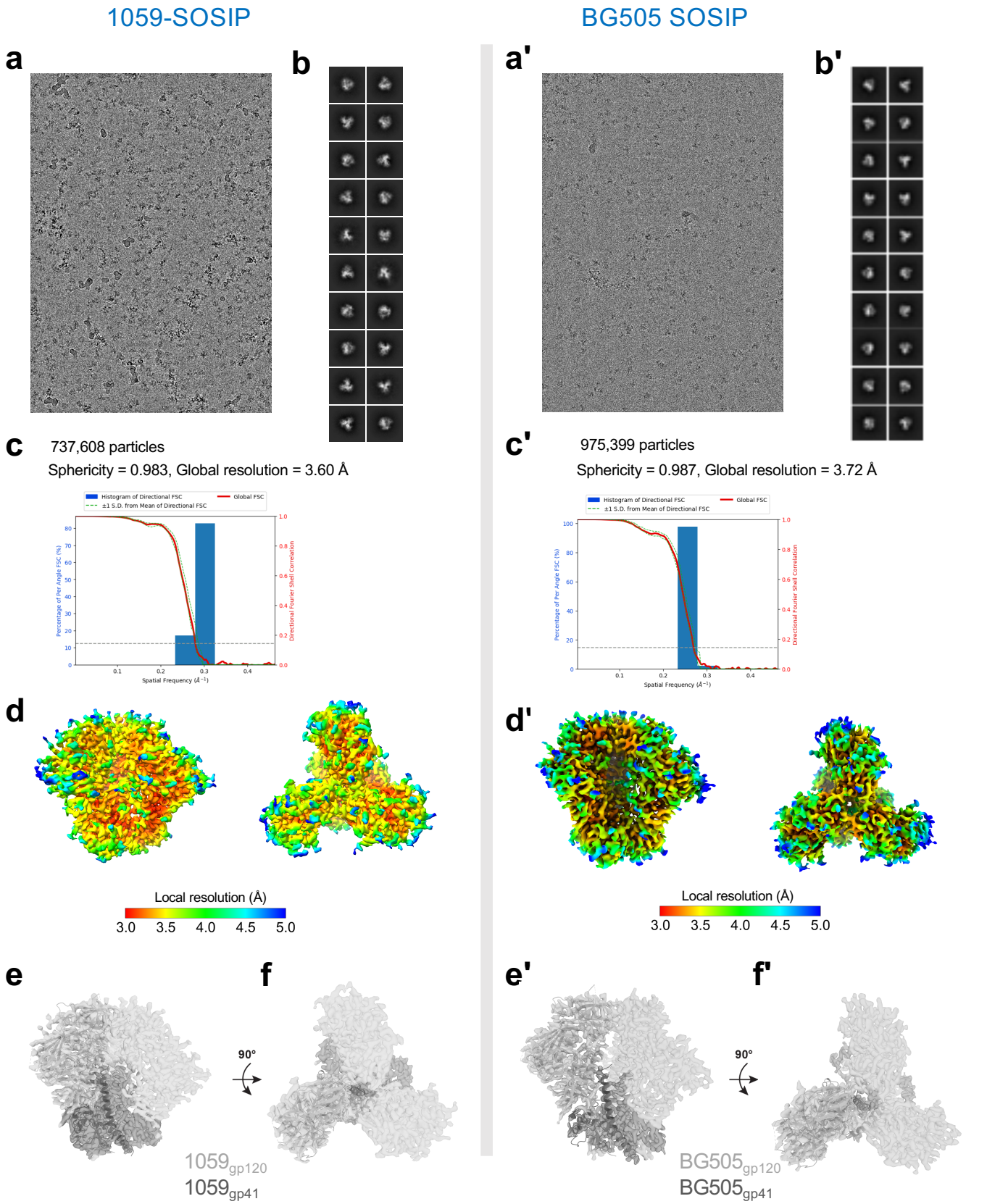

Extended Data Fig. 6. Summary of cryo-EM data processing and validation of unliganded 1059 (left) and reference control unliganded BG505 (right) SOSIPs. a,a', Representative micrograph and **b,b',** cryo-EM 2D class averages for 1059 or BG505 SOSIP cryo-EM data collection. **c,c'**, Gold-standard Fourier shell correlation (FSC) plot for the map. Estimate is reciprocal of spatial frequency at Fourier shell correlation value of 0.143 (horizontal dashed line). **d,d',** Local resolution estimation of the 1059 / BG505 SOSIPs. **e-f,e'-f',** Side and top views of rigid body fit for one protomer of an Env trimer from the BG505-IOMA-10-1074 model (PDB 5T3Z; IOMA and 10-1074 Fabs removed) shown in cartoon and SOSIP cryo-EM densities.

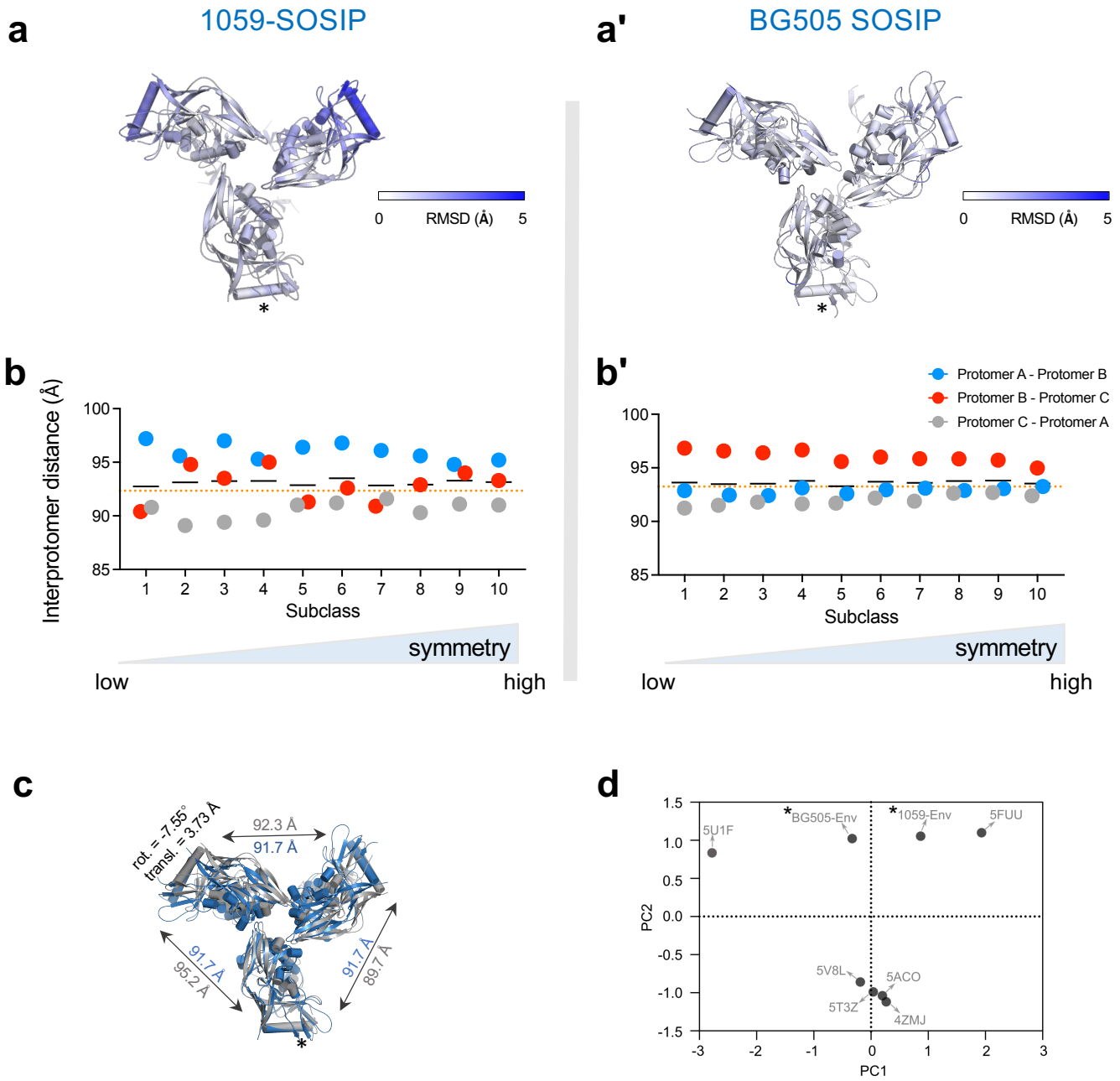

Extended Data Fig. 7. Conformational flexibility and asymmetry of 1059-SOSIP. a,a', We assessed motions of protomers in 1059 and BG505 SOSIP Envs by measuring the distance between each residue in the 2 most distanced subclasses (out of 10 shown in Fig. 2b) of each SOSIP (i.e. 2 subclasses with the highest Cα root mean square deviation between them). The Env residues were colored according to the distance between same residue in the two chosen conformations. Data processing for generating these subclasses in described in the Methods section. Number of particles used, and resolution of each sub-class model are provided in Extended Data Table 4. **b,b'**, Interprotomer distance analysis of the 10 sub-classes shown in Fig. 2b. Distances was measured between residue 343 (HXBc2 numbering corresponding to Arg in 1059-SOSIP or Gly in BG505-SOSIP) of different protomers, and the sub-classes were ordered according to their symmetry based on the sum of differences of the interprotomer distances from the geometric mean of the interprotomer distances as described in the Methods section. **c**, Unliganded, incompletely closed 1059-SOSIP structure (colored gray) overlaid on the structure of a perfectly symmetric unliganded HIV-1 Env SOSIP crystal structure (PDB: 4ZMJ; colored blue). An asterisk indicates the protomer used for superposition; we evaluated 1059-SOSIP asymmetry from misalignment of the other two protomers of the 1059-SOSIP (gray) with the corresponding protomers of the symmetric reference structure (blue). **d,** Principal component analysis of interprotomer distances in different soluble Envs. *, SOSIP structures solved in this study by cryo-EM and refined with C1 symmetry.

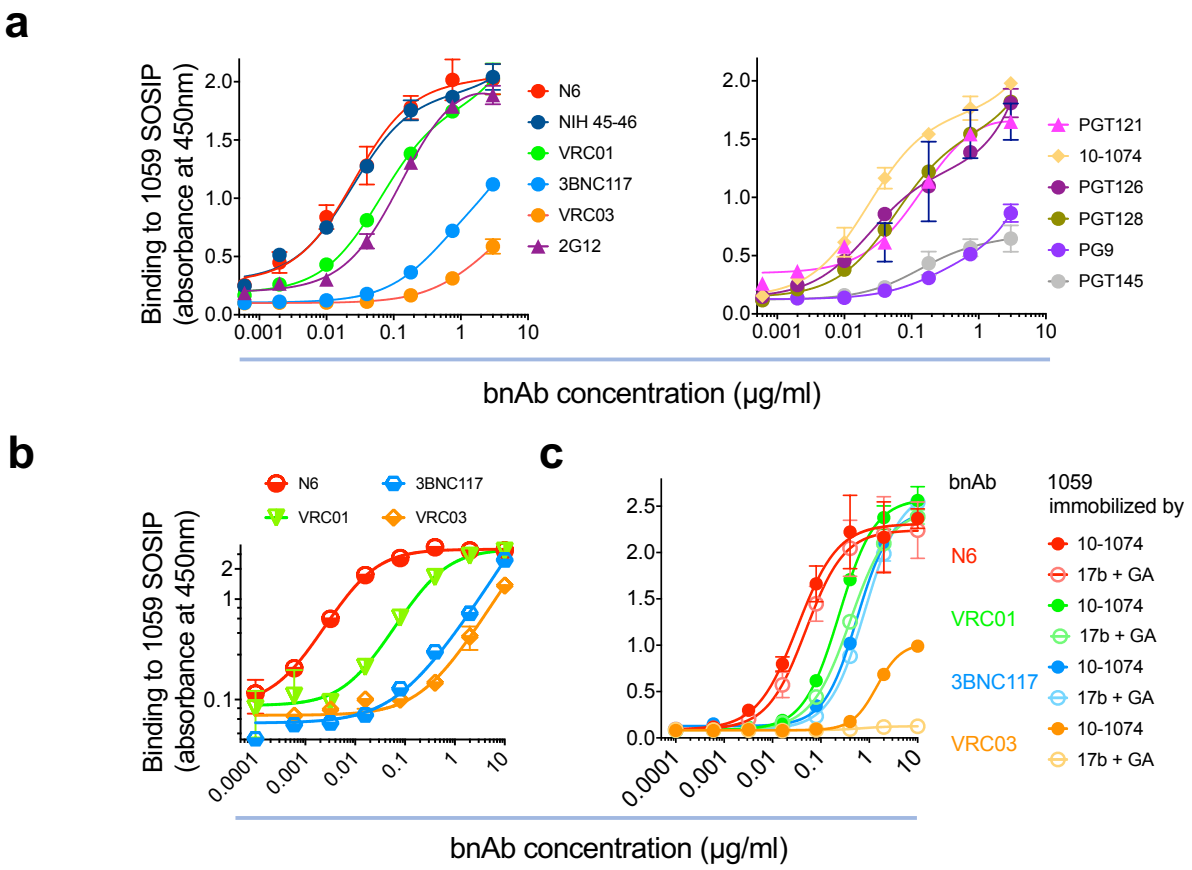

Extended Data Fig. 8. Antibody binding to soluble SOSIP trimers. a, We measured bnAb binding to directly immobilized soluble 1059 SOSIP trimer by ELISA using anti-human IgG conjugated to HRP. **b-c**, Binding of CD4bs bnAbs to 1059 SOSIP immobilized by *Galanthus nivalis* lectin (**b**), 10-1074 (**c;** closed circles) or 17b and crossed linked (**c** open circles). Data are representative of at least 2 independent experiments, each performed at least in duplicate.

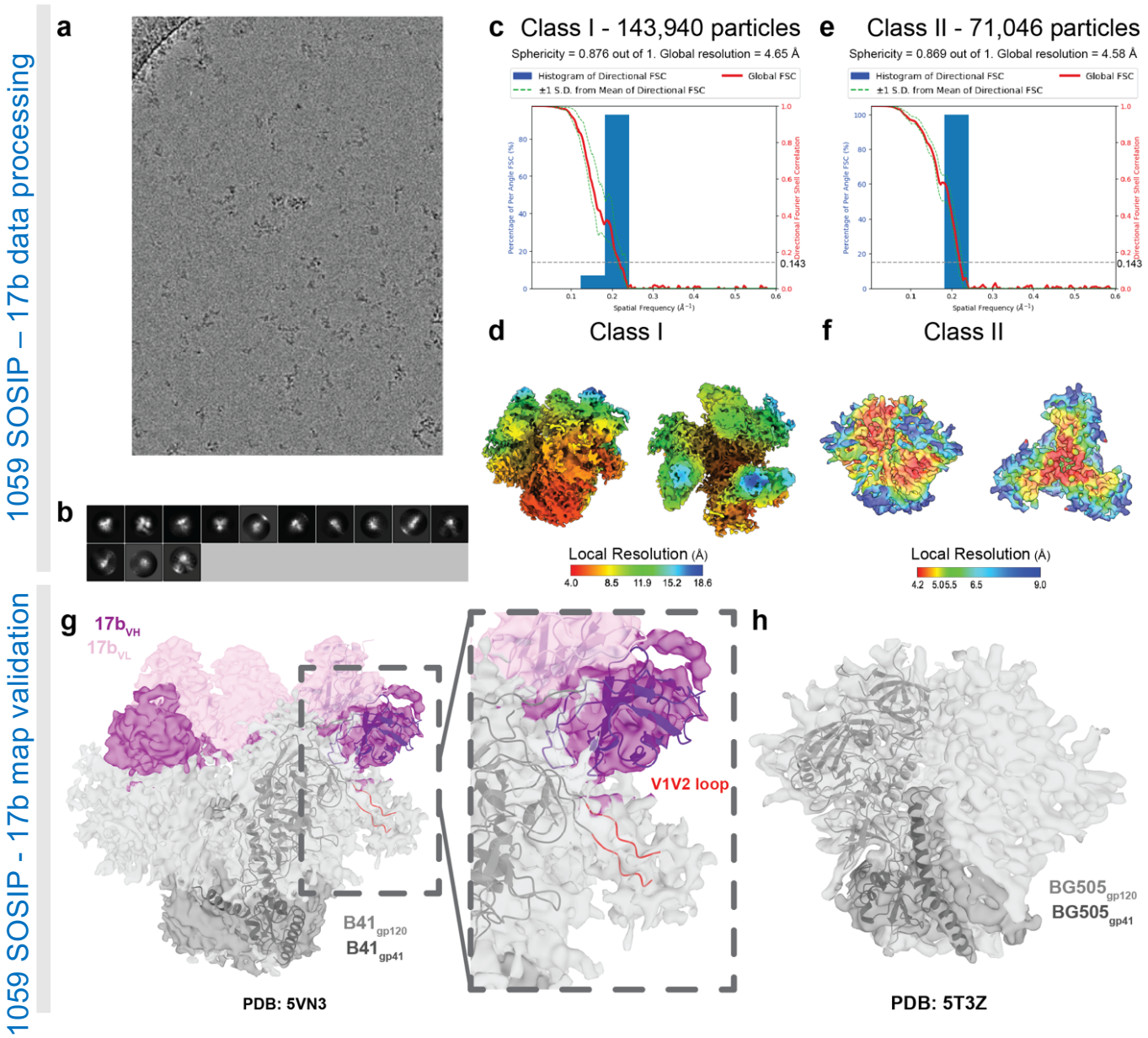

Extended Data Fig. 9. **Summary of 1059 SOSIP - 17b cryo-EM data processing, validation, and further interpretation a,** Representative micrograph and **b,** cryo-EM 2D class averages for 1059 SOSIP - 17b cryo-EM data collection. Gold-standard Fourier shell correlation (FSC) plots for class I – 1059 SOSIP - 17b complex **(c,d)** and the class II – 1059 SOSIP (unliganded) **(e,f)**. Estimate is reciprocal of spatial frequency at Fourier shell correlation value of 0.143 (horizontal dashed line). **d-f,** Local resolution estimation of 1059 SOSIP-17b complex (**d**) and unliganded 1059 SOSIP (**f**). **g** Rigid body fit for one protomer of the B41-17b-sCD4 model shown in cartoon (PDB: 5VN3, sCD4 not shown) in class I 1059 SOSIP - 17b EM density (left). Zoomed-in panel showing ordered portions of the displaced V1V2 loop fit in density in red (right). **h** Rigid body fit for one protomer of a Env trimer from the BG505-IOMA-10-1074 model (PDB: 5T3Z, IOMA and 10-1074 not shown) shown in cartoon and class II 1059 SOSIP cryo-EM density.

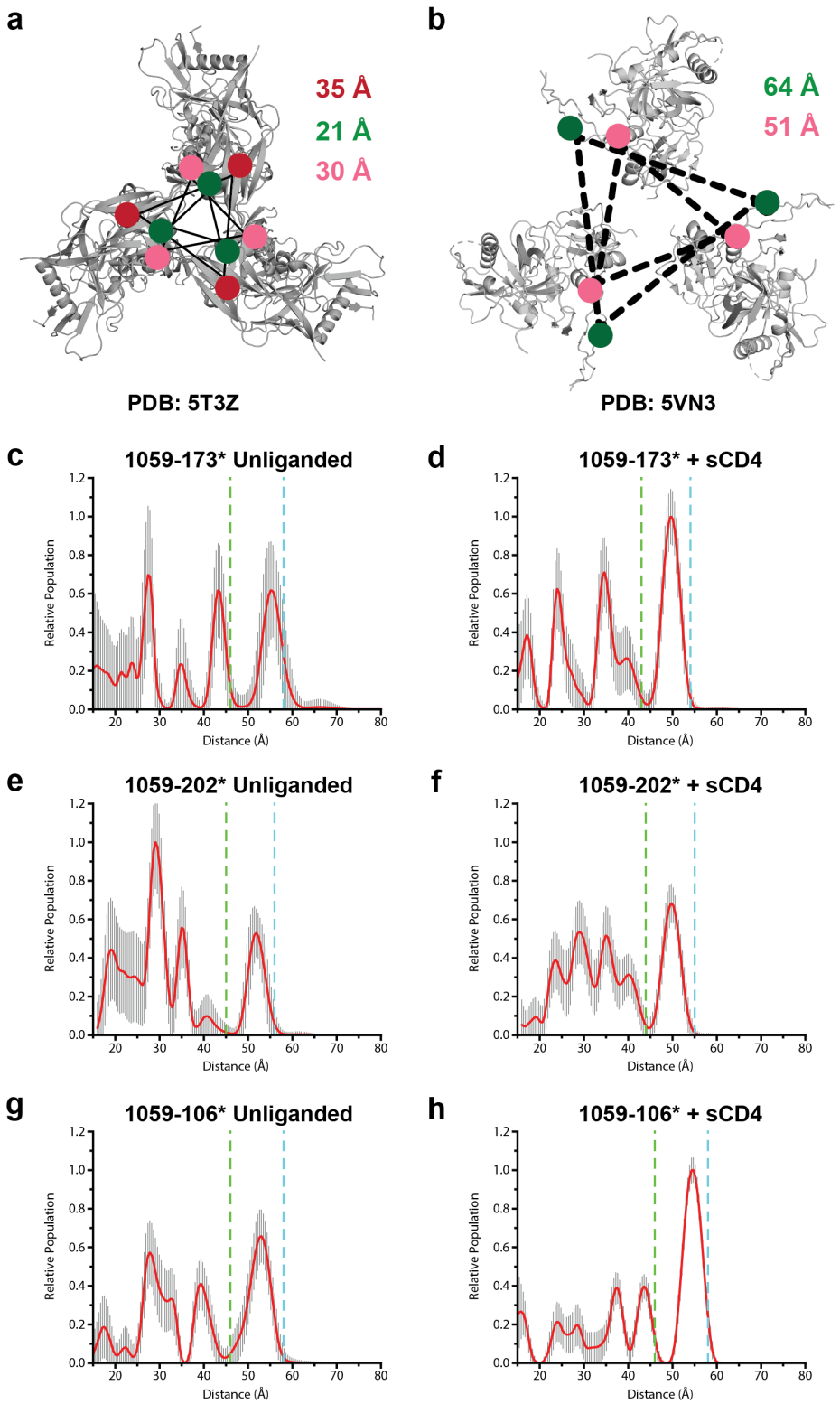

Extended Data Fig. 10. SOSIP distance measurements and DEER distance distribution error analysis. a, Distance between Cα atoms at labeled residues 173 (red), 202 (green), and 106 (pink) measured on a SOSIP Env structure (PDB: 5CEZ) and represented as circles. **b,** Similar to (**a)** but on an sCD4-bound SOSIP Env structure (PDB: 5VN3). Distance measurements for labeled residue 173 are not shown for sCD4-Env structure because this residue was disordered. **c-h,** Results from the "Errors" module in LongDistances DEER analysis software for distance distributions shown in Fig. 2f. This error analysis algorithm provides a conservative estimate of confidence in the distance distributions, with the following parameters used in the analysis: model-free smoothness = 10, additional noise = 1 x sd, background noise = 0.1 x sd. Despite the low signal-to-noise ratios and modulation depths seen for the data, these plots confirm unequivocal structural changes resulting from the addition of sCD4. Green and blue vertical dashed lines indicate the Jeschke confidence limits for peak shape and position, respectively (Ref[40]).

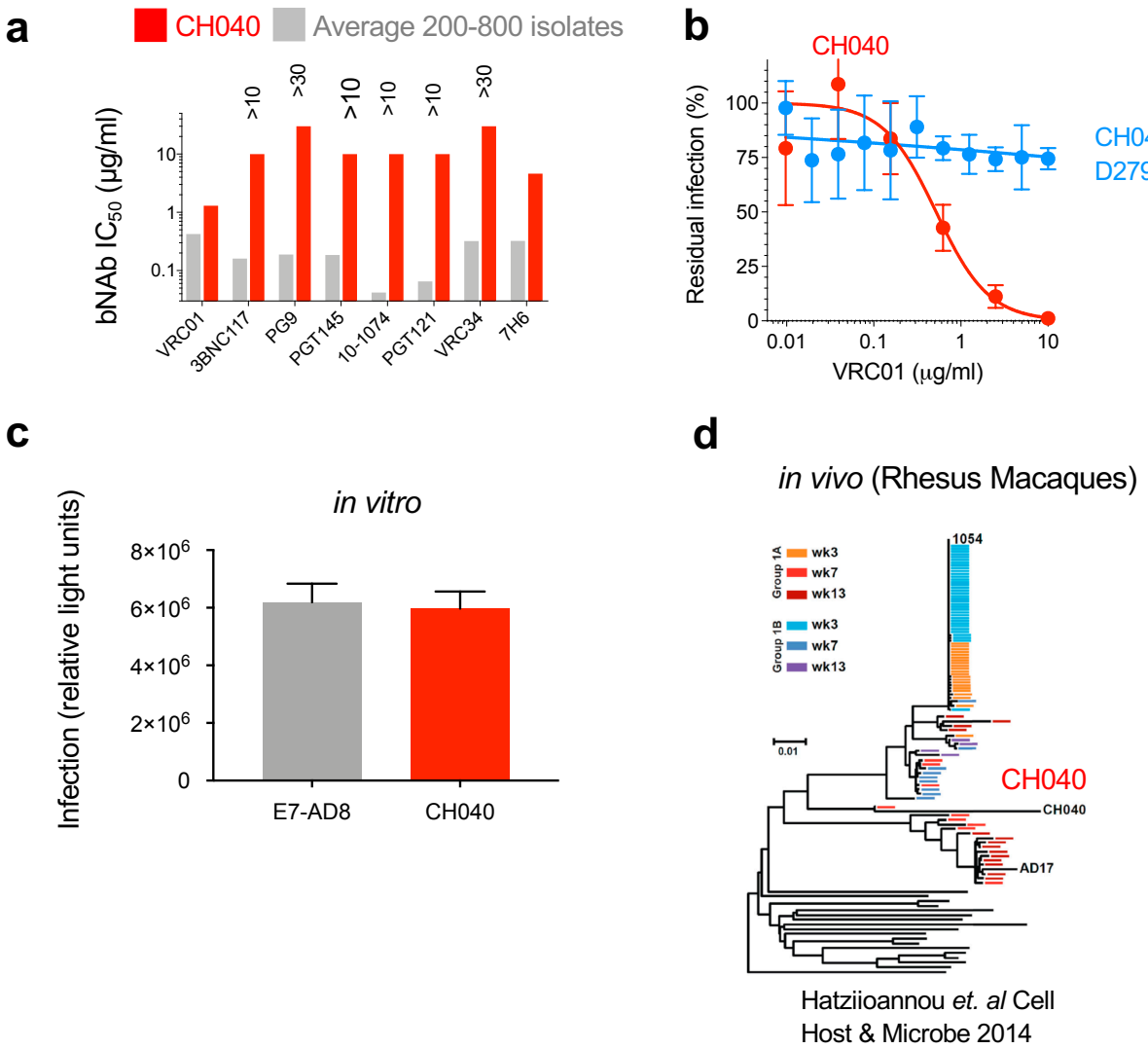

Extended Data Fig. 11. CH040 Env sensitivity to bnAbs and CH040 Env function. a, Comparison of CH040 Env sensitivity (red) and the average sensitivity of 200-800 Envs of different HIV-1 strains (grey) to bnAbs. Data for the sensitivity of different Envs to bnAbs were retrieved from the HIV-1 database (www.hiv.lanl.gov) and compared to the IC_{50}s shown in Extended Data Fig. 3. **b,** Introduction of the E279D change to CH040 Envs conferred HIV-1 resistance to VRC01 (up to 10 µg/ml). **c,** CH040 Env-mediated entry *in vitro* is comparable to the Env-mediated entry of the primary isolate AD8. **d,** CH040 efficiently replicates *in vivo* in rhesus macaques (adapted from Hatziioannou *et. al.* Cell Host & Microbe 2014).

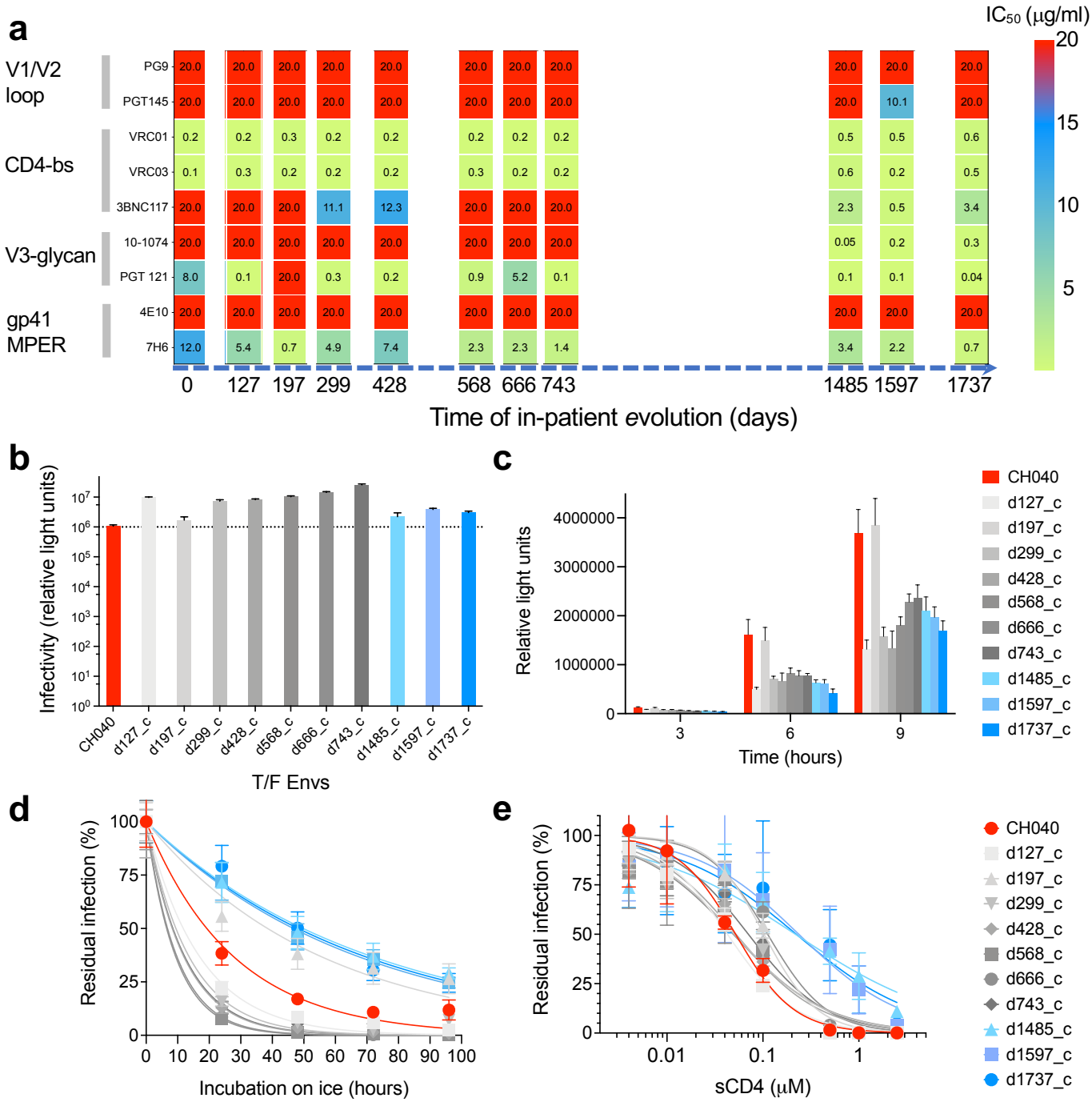

Extended Data Fig. 12. Reconstructing the evolutionary pathways of (preexisting) multi-bnAb resistant T/F strain (CH040) in infected individual. a, Sensitivity of viruses pseudotyped with reconstructed consensus Envs to bnAbs targeting the five known sites of Env vulnerability. Envs from 10 different time points (day 127 to day 1737) were reconstructed based on consensus sequences after alignment and analysis of all available sequences for each time point (see Extended Data Table 4 and Supplementary Table 2). Indicated values are IC_{50s} in μg/ml and were used for Fig. 3d plots. **b,** Infectivity levels of reconstructed-Env pseudoviruses; 2ng p24 of each pseudovirus were used to infect Cf2Th-CD4/CCR5 target cells. For CH040, 2.5 ng p24 was used and the measurements were normalized to 2 ng p24. **c,** Cell-cell fusion activity. Env-expression plasmids of specified Envs were co-transfected with Tat-expression plasmid (5:1 Env:Tat ratio) into 293T cells and after 48-hours transfected cells were detached with PBS/5mM EDTA and incubated with TZM-bl cells. Extent of fusion was measured by firefly luciferase activity, which is expressed in the fused cells by Tat-mediated activation and used as a reporter. **d-e,** Sensitivity of reconstructed-Env pseudoviruses to cold exposure (**d**) and to sCD4 (**e**). Color codes for panels (**d**) and (**e**) are identical and shown on the right. Data shown are the average (**a**, **d** and **e**) or representative (**b** and **c**) results of at least two independent experiments each performed in duplicate or quadruplicate; mean relative light units or residual infection ± SD are reported (**b-e**).

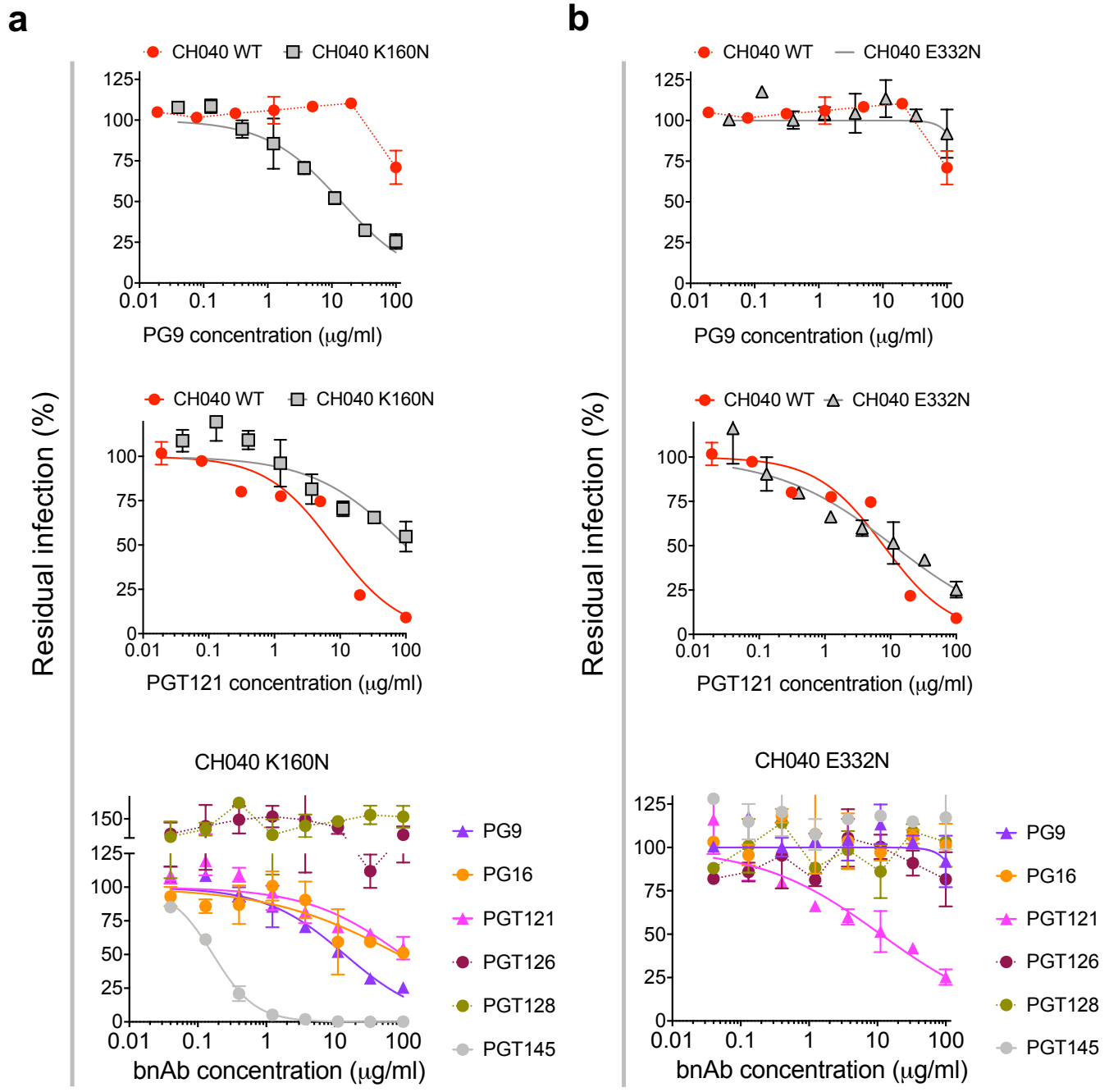

Extended Data Fig. 13. Sensitivity of K160N and E332N variants of CH040 Env to different bnAbs. Effects of bnAbs targeting gp120 V1/V2 loop (PG9, PG16, and PGT145) and bnAbs targeting gp120 V3 glycan (PGT 121, PGT126, and PGT128) on the entry of pseudoviruses displaying the K160N (**a**) and E332N (**b**) CH040 Env variants. Data shown (mean ± SD) are representative results from one of at least 2 independent experiments performed in duplicate.

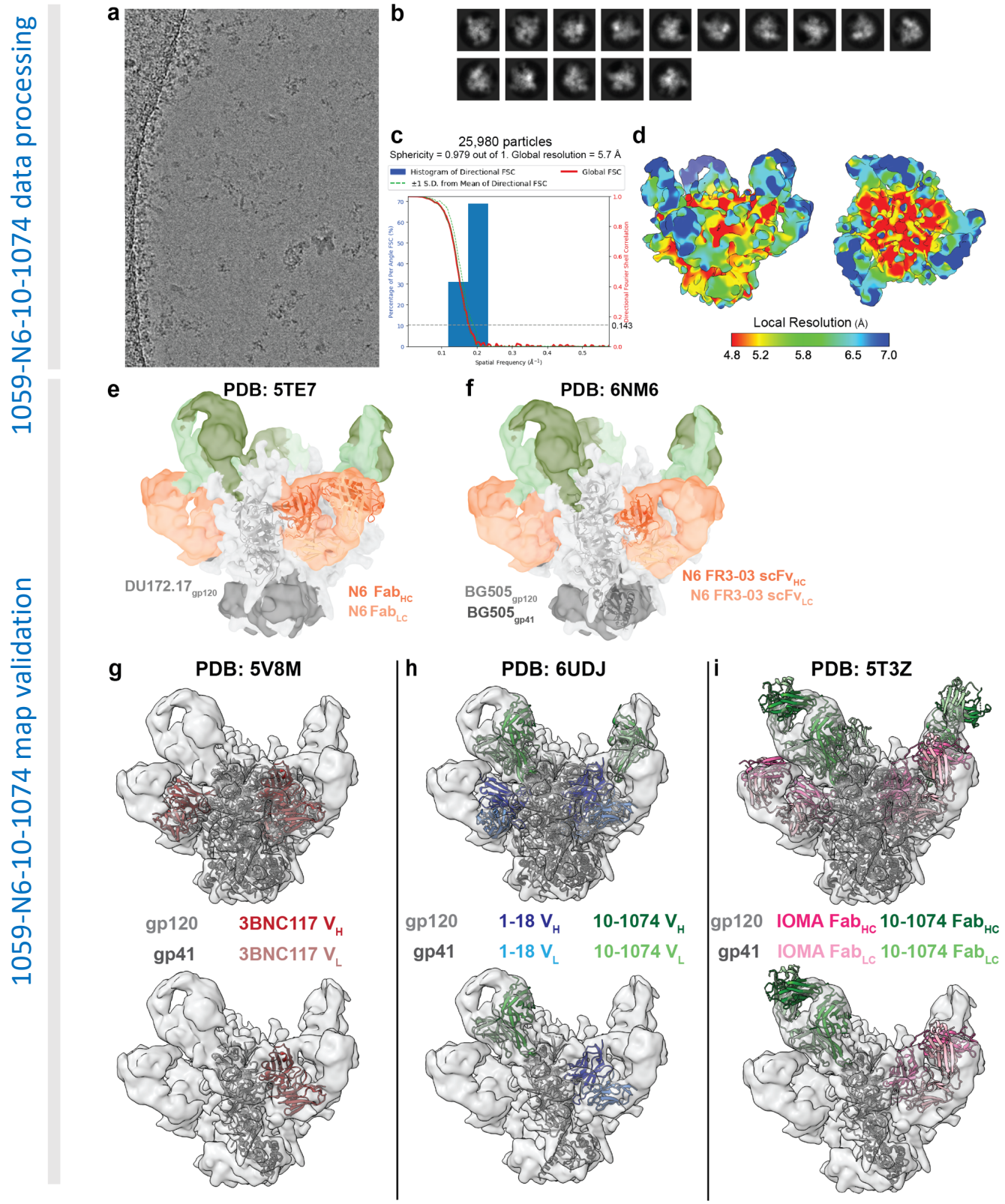

Extended Data Fig. 14. Summary of 1059 SOSIP - N6 - 10-1074 cryo-EM data processing, validation, and further interpretation a, Representative micrograph and **b,** cryo-EM 2D class averages for 1059SOSIP-N6-10-1074 cryo-EM data collection. **c,** Gold-standard Fourier shell correlation (FSC) plot was used to estimate structure global resolution of 1059SOSIP-N6-10-1074 complex. Estimate is reciprocal of spatial frequency at Fourier shell correlation value of 0.143 (horizontal dashed line). **d,** Local resolution estimation for the 1059SOSIP-N6-10-1074 complex. Rigid body fits of a protomer for DU172.17 gp120-N6 (PDB: 5TE7) **(e)** and BG505-N6 FR3-03 scFV-3H109 Fab-35022 scFV (PDB: 6NM6, 3H109 Fab and 35022 scFv not shown) **(f)** shown in cartoon in 1059SOSIP-N6-10-1074 EM density. **g-i,** Rigid body fits of trimers (top) and protomers (bottom) for structure models of BG505-3BNC117 (PDB: 5V8M) (**g**), BG505-1-18-10-1074 (PDB: 6UDJ) (**h**), and BG505-IOMA-10-1074 (PDB:5T3Z) (**i**)**.** Fits are shown in cartoon in 1059SOSIP-N6-10-1074 EM density map.

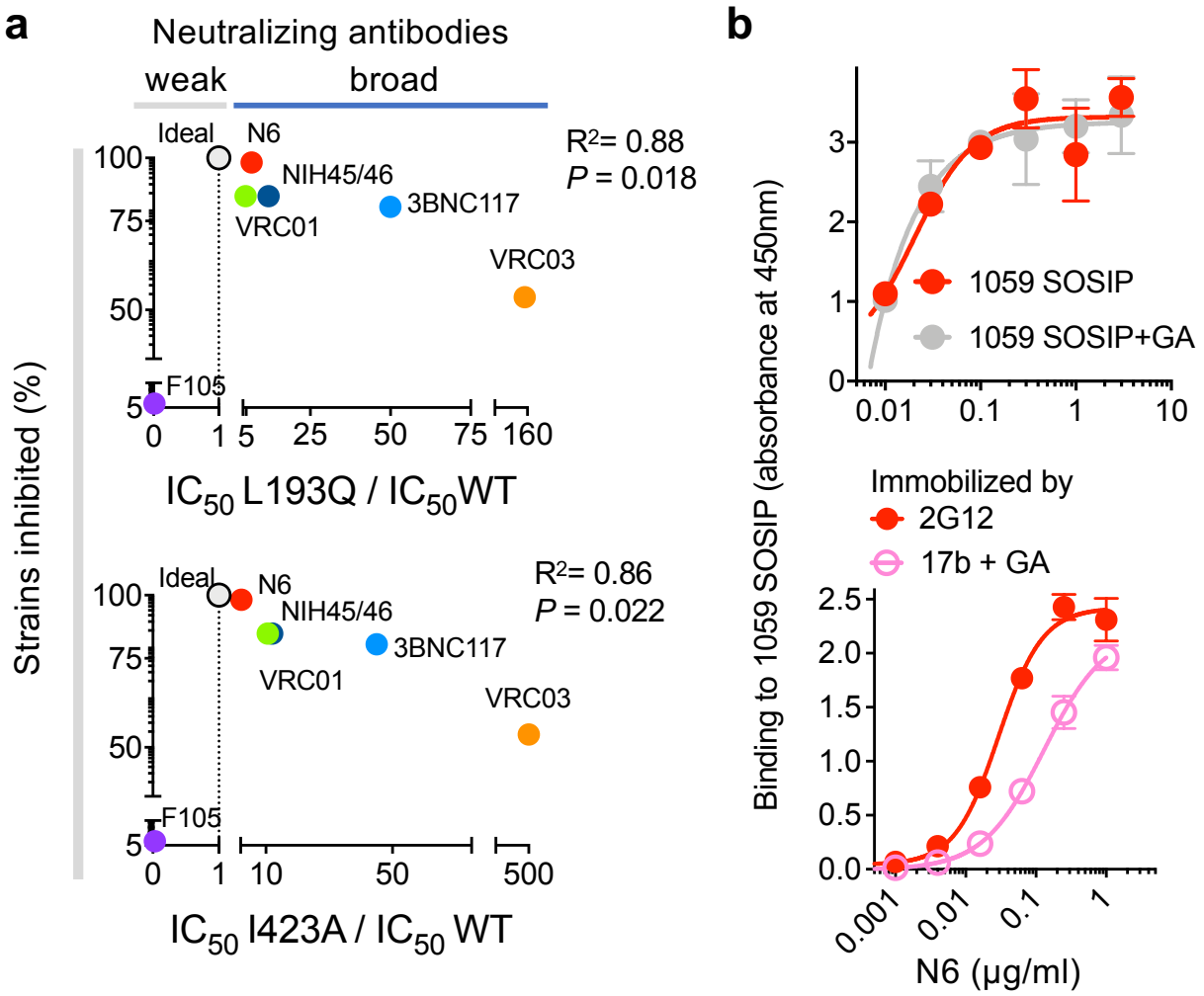

Extended Data Fig. 15. Recognition of multiple HIV-1 Env conformations by CD4bs antibodies. **a,** Comparison between breadth and efficiency to neutralize multiple Env conformation of broadly and weakly CD4bs neutralizing antibodies. Top - relationship between the breadth of CD4bs neutralizing antibodies and efficiency to neutralize HIV-1_{JRFL} Env functional intermediate L193Q. Bottom – same as top but for the efficiency to neutralize HIV-1_{JRFL} Env open conformation (I423A). These plots extend those of Fig. 4d (middle and right) and show the position of an ideal bnAb and of the weakly neutralizing antibody F105. **b, Top,** Comparison of N6 binding to 1059 SOSIP that was crosslinked by glutaraldehyde (GA) to restrict Env transitions and the binding to non-crosslinked 1095 SOSIP. **Bottom,** Comparison of N6 binding to 1059 SOSIP that was immobilized via 2G12 antibody and 1059 SOSIP immobilized by 17b antibody and further crosslinked by GA to stabilize open Env conformation.

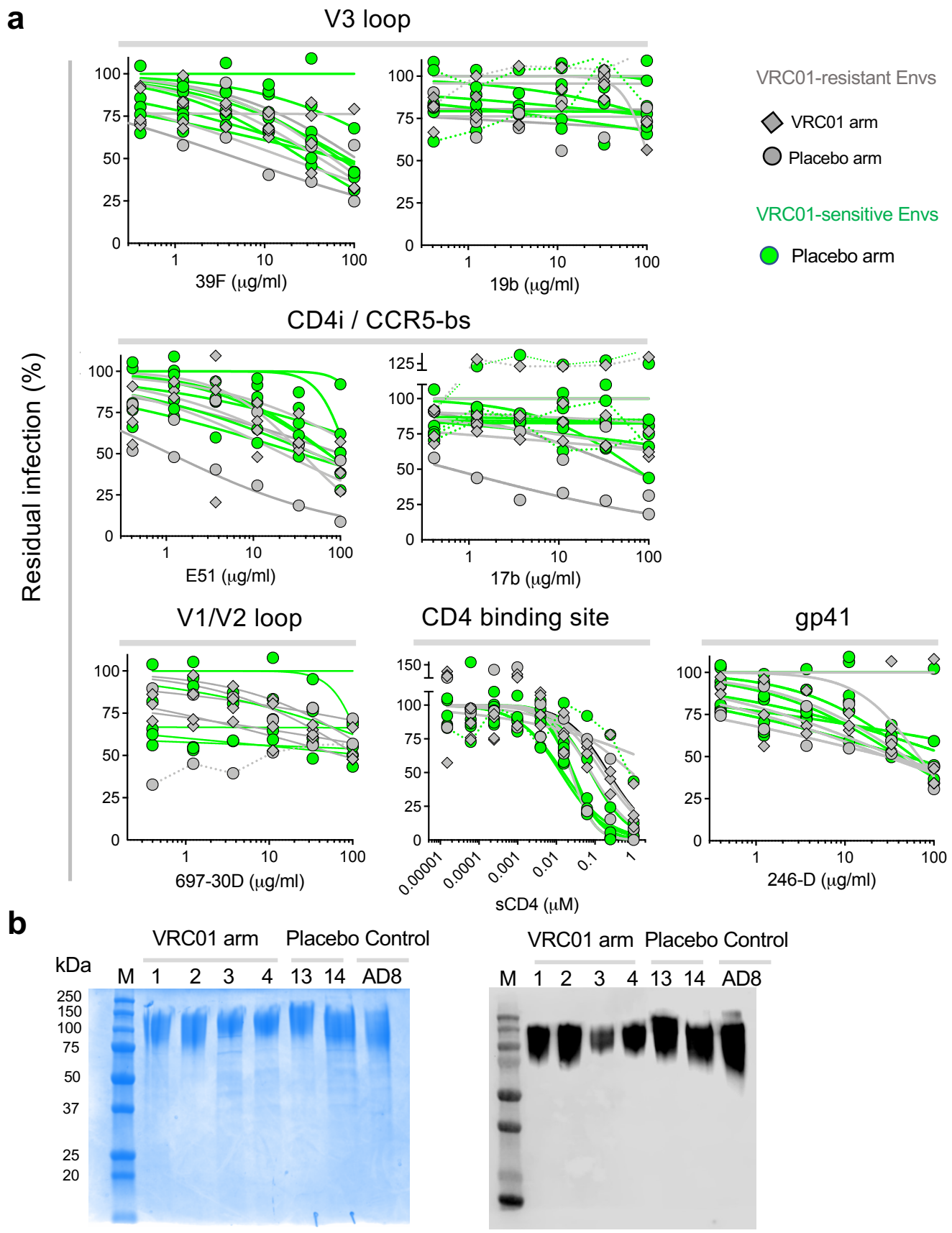

Extended Data Fig. 16. Sensitivity of HIV-1 Envs, isolated from the antibody (VRC01)-mediated prevention (AMP) trial, to different Env ligands that preferentially neutralize Env open conformation and gp120 expression of Envs from VRC01-resistant strains. a, Sensitivity of VRC01-resistant (grey) and VRC01-sensitive Envs (green) to internal-epitope antibodies and soluble CD4. Results are the average of 2-5 independent experiment, each performed in 2-4 replicates. **b,** SDS-PAGE (left) and western blot (right) of gp120 of VRC01-resistant HIV-1 strains. gp120 IDs are the same as those used in Fig. 5f-g.

Extended Data Table 1

	Closed	Functional intermediates*	Open
Cold exposure	Resistant	Sensitive	Sensitive
sCD4 / CD4 mimetics	Moderately sensitive	Sensitive	Hypersensitive
Conformational blockers	Hypersensitive	Moderately resistant	Resistant
CD4-independent infection	Low	Moderate	Relatively high
VRC01	Sensitive	Relatively resistant	Resistant
VRC03	Sensitive	Relatively resistant	Resistant
3BNC117	Sensitive	Relatively resistant	Resistant
4E10	Moderately sensitive	Sensitive	Hypersensitive
7H6	Sensitive	Sensitive	Hypersensitive
PGT151	Sensitive	Sensitive	Hypersensitive
VRC034	Relatively sensitive	Sensitive	Sensitive
PG9	Sensitive	Relatively resistant	Resistant
17b	Resistant	Relatively sensitive	Sensitive
19b	Resistant	Relatively sensitive	Sensitive
Patient serum	Generally resistant	Sensitive	Hypersensitive
T20	Sensitive	Sensitive	Hypersensitive

*By definition an intermediate phenotype can result from intermediate sensitivity to Env ligands that target internal epitopes or to cold, or it can result from sensitivity to some of these ligands/cold. In addition, resistance to a specific inhibitor can be the result of changes in the epitope/binding site and not necessary changes in Env conformation but resistance of multiple molecules targeting the same site is likely related to conformational changes.

Extended Data Table 2. HIV-1 transmitted/founder Envs.

#	Env ID*	Env clone**	Tier	Fiebig Stage	Accession Number
1	1012	p1012.TC21.3257	1B or 2	III	EU289184
2		p1006_11.C3.1601	2	III	EU289183
3	1054	p1054.TC4.1499	2	II	EU289185
4		p1056.TA11.1826	1B or 2	II	EU289186
5	1058	p1058_11.B11.1550	2	IV	EU289187
6	1059	p1059_09.A4.1460	2	III	EU289188
7		p62357_14.D3.4589	2	II	EU289189
8	6244	p6244_13.B5.4567	2	II	EU289191
9		p6240_08.TA5.4622	2	II	EU289190
10	63358	p63358.p3.4013	2	II	EU289192
11	CH040***	p700010040.C9.4520	2	II	EU289193
12		p700010058.A4.4375	2	III	EU289194
13		p9014_01.TB1.4769	2	II	EU289195
14	9021	p9021_14.B2.4571	2	II	EU289196
15	PRB926	pPRB926_04.A9.4237	2	II	EU289197
16		pPRB931_06.TC3.4930	2	III	EU289198
17	PRB958	pPRB958_06.TB1.4305	2	III	EU289199
18	SC05	pSC05.8C11.2344	2	II	EU289200
19	SC45	pSC45.4B5.2631	2	II	EU289201
20	WEAU	pWEAUd15.410.5017	2	II	EU289202

* Env ID is shown for the 13 T/F Env clones that were selected for testing in the current study
** All Env-expressing plasmids (Env clones) of T/F strains were kindly provide by Drs. Beatrice H. Hahn, Brandon F. Keele and George M. Shaw through the NIH AIDS Reagent Program
*** An infectious molecular clone is available (pCH040.c/2625; Catalog number 11740); subject identifier 700010040

Extended Data Table 3. Cryo-EM data collection, refinement and validation statistics of SOSIP Env structures.

	1059	BG505	1059-17b (class I)	1059 (class II)	1059-N6-10-1074
PDB ID	8TGW	8TGU			
EMDB ID	41246	41244	26264	26265	26266
Data Collection and processing					
Microscope	FEI Titan Krios				Talos Artica
Detector	Gatan K3				
Magnification	x81000		x105000		x45,000
Voltage (kV)	300				200
Electron exposure (e-/Å^2)	59.1	63.2	60		
Defocus Range (μm)	1.0-3.0	1.4-1.8	1.0-3.0		
Pixel size (Å)	1.08		0.855		0.869
Reconstruction software	cryoSPARC		RELION		cryoSPARC
Symmetry imposed	C1		C3		
Movies	13,405	14,296	10,738		2,744
Initial particle images (no.)	7,260,519	6,566,700	2,168,339	676,453	317,131
Final particle images (no.)	737,588	975,399	143,940	71,046	25,980
Map resolution (Å)	3.6	3.7	4.7	4.6	5.7
Initial model used	ab-initio	ab-initio	auto-refinement		ab-initio
FSC threshold	0.143				
Coordinate Refinement					
Model resolution (Å)	3.6	3.7			
FSC threshold	0.5				
Model composition					
Nonhydrogen atoms	13,449	14,880			
Protein residues	1,488	1,719			
R.M.S. deviations					
Bond lengths (Å)	0.005	0.004			
Bond angles (°)	0.789	0.703			
Validation					
MolProbity score	1.14	1.33			
Clashscore	1.61	1.84			
Poor rotamers (%)	0	0			
Ramachandran plot					
Favored regions (%)	96.44	94.26			
Allowed (%)	3.49	5.68			
Disallowed regions (%)	0.07	0.06			

Extended Data Table 4. Subclassification of unliganded 1059 and BG505 SOSIP cryo-EM datasets.

Unliganded 1059 SOSIP			Unliganded BG505 SOSIP		
Class ID	Particles	Resolution (Å)	Class ID	Particles	Resolution (Å)
1	53,177	3.93	1	84,089	4.16
2	71,533	3.79	2	64,582	4.22
3	57,181	3.82	3	69,147	4.24
4	57,278	3.96	4	81,171	4.14
5	45,804	4.04	5	278,726	3.93
6	69,801	3.74	6	86,261	4.11
7	57,124	4.06	7	85,273	4.14
8	50,430	4.01	8	79,022	4.22
9	55,435	4.12	9	81,500	4.18
10	219,825	3.72	10	65,628	4.23
Total	737,588		Total	975,399	

Extended Data Table 5. Constructing consensus HIV-1 Env sequences of 10 time points during in-patient evolution of CH040.

	Time points (days)*															
	<16	d16	d32	d61	d127**	d197	d299	d428	d568	d666	d743	d1485	d1513	d1569	d1597	d1737
# seq available	7	22	33	28	67	32	39	37	34	45	25	30			35	41
Dominant changes (>50% strains except when indicated)	none	none	none	none												
									G135E	G135E						
									N136K	N136K						
										V137G (49%)						
								N139T			N139T	N139T				N139T
																N142M
																S143G
							N144K		N144T							
									G146E			G146E			G146E	G146E
					E147K	E147G		E147T	E147K		E147T	E147T			E147T	E147T
								M148L			M148L	M148L			M148L (inset)	
												K160R			K160R	K160R
									I165V			I165M			I165M	I165M
												K166Q			K166Q	K166Q
															R-to-S (188?)	
												I234N			I234N	I234N
							T295N		T295N	T295N	T295N	T295N			T295N	T295N
							N300H		N300H	N300H	N300H					
												P308H			P308H	P308H
												D321A			D321G	D321A
								T323I	T323I	T323I	T323I	T323I			T323I	T323I
						R327K										
								Y330S				Y330H			Y330H	Y330H
						E332K		E332K				E332N			E332N	E332N
												N334S			N334S	N334S
															S340N	
										E347G						
										Q352K						
															R363H	R363H
															W401G	
												K405E			K405N	K405N
															D409N	
								G412D		G412D						
								I415M		I415M		I415T			I415T	I415T
									K419R	K419R	K419R	K419R			K419R	K419R
																G429E
								K442I	I422E (42%)	I442Q (48%)	K442I	K442I			K442I	K442I
												R444K			R444K	R444K
												E463K			E463K	E463K
															D636N	D636N
															L663W	
															L721F	
							A754T	A754T	A754T	A754T		A754T			A754T	A754T
															V778A	
												R770H				
															N809K	
							I820T	I820T	I820T	I820T						
												C837G			C837G	C837G
												L841R			L841R	L841R

* Sequences from 10 time points highlighted in yellow were used for reconstruction of consensus viruses
** Consensus of sequences from day 127 and day 148 contained a single change and they were combined

Extended Data Table 6. HVTN 704 HIV-1 Envs.

#	Env ID	Env clone ID**	Arm	VRC01
1	1	H704_3083_040_EsN	VRC01	Resistant
2	2	H704_2625_090EsN		
3	3	H704_1481_220_RE_p002s		
4	4	H704_2643_210_RE_p001s		
5	6	H704_2536_030_RE_p003s	Placebo	Sensitive
6	7	H704_1747_170_RE_con_s		
7	8	H704_0011_240_RE_pb002_s		
8	9	H704_0011_240_RE_pb003_s		
9	10	H704_0011_240_RE_pb001_s		
10	11	V704_1350_750_RE_pbsga001_s		
11	12	H704_1969_210_RE_pbsga002_s		
12	13	H704_1835_150_RE_p002s_2484A		Resistant
13	14	H704_0445_180_RE_con_s		

** All Env-expressing plasmids (Env clones) of AMP HIV-1 strains were kindly provide by Dr. David Montefiori, Duke University.